EUROPEAN ORGANIZATION FOR NUCLEAR RESEARCH

CERN/EP 89-101
15 August 1989

ELECTROWEAK PARAMETERS FROM A HIGH STATISTICS NEUTRINO NUCLEON SCATTERING EXPERIMENT

A. Blondel, P. Böckmann[1], H. Burkhardt, F. Dydak, A.L. Grant, R. Hagelberg, E.W. Hughes[2], W. Krasny[3], A. Para[4], H. Taureg, H. Wachsmuth and J. Wotschack
CERN, Geneva, Switzerland

H. Blümer[5], H.D. Brummel[5], P. Buchholz[6], J. Duda, B. Kampschulte, K. Kleinknecht[5], J. Knobloch[7], E. Müller[5] and B. Renk[5]
Institut für Physik(*) der Universität, Dortmund, Fed. Rep. Germany

R. Belusevic, B. Falkenburg, R. Geiges, C. Geweniger[7], V. Hepp, H. Keilwerth and K. Tittel
Institut für Hochenergiephysik der Universität, Heidelberg
Fed. Rep. Germany

H. Abramowicz[8], C. Guyot, J.P. Merlo, P. Perez, F. Perrier, J.P. Schuller, R. Turlay and B. Vallage
DPhPE, CEN - Saclay, France

J. Królikowski[7] and A. Lipniacka
Institute of Experimental Physics(**), University of Warsaw, Poland

1 Now at DESY, Hamburg, Fed. Rep. of Germany
2 Now at Siegen University, Siegen, Germany
3 Now at Inst. of Nucl. Physics, Krakow, Poland
4 Now at Fermilab, Batavia, USA
5 Now at Inst. für Physik, Univ. of Mainz, Mainz, Fed. Rep. of Germany
6 Now at Temple University, Philadelphia, PA, USA
7 Now at CERN, Geneva, Switzerland
8 Now at Inst. of Experimental Physics, Warsaw, Poland

Submitted to Zeitschrift für Physik C

(*) Supported by the Bundesministerium für Forschung and Technologie, Bonn, Fed. Rep. Germany.

(**) Supported by the Polish Ministry of Education, grant CPBP01.06.

EP/4301P/HW/mk

ABSTRACT

The final results from the WA1/2 neutrino experiment in the 1984 CERN 160 GeV narrow band beam are presented. The ratios R_ν and $R_{\bar{\nu}}$ of neutral to charged current interaction rates of neutrinos and antineutrinos in iron are measured to be $R_\nu = 0.3072 \pm 0.0033$ and $R_{\bar{\nu}} = 0.382 \pm 0.016$. A value of the electroweak parameter $\sin^2\theta_W = 1 - m_W^2/m_Z^2$ is extracted from R_ν. The result is $\sin^2\theta_W = 0.228 + 0.013\ (m_c - 1.5) \pm 0.005$ (exp.) ± 0.003 (theor.) where m_c is the mass of the charmed quark in GeV for $m_t = 60$ GeV, $m_H = 100$ GeV, $\rho = 1$. Combining R_ν and $R_{\bar{\nu}}$, one obtains a value for $\rho = 0.991 + 0.023\ (m_c - 1.5) \pm 0.020$ (exp.). Alternatively, R_ν and $R_{\bar{\nu}}$ yield a precise value of the ratio of intermediate vector boson masses $m_W/m_Z = 0.880 - 0.007\ (m_c - 1.5) \pm 0.002$ (exp.) ± 0.002 (theor.). Comparison of these results with those from direct measurements of the vector boson masses are presented. In a model-independent analysis the left-and right-handed neutral current coupling constants, g_L^2 and g_R^2, are determined.

1. INTRODUCTION

A detailed account is given of the 1984 WA1/2 neutrino and antineutrino nucleon scattering experiment, a first result of which: $\sin^2\theta_W = 0.225 \pm 0.005(\text{exp.}) \pm 0.003(\text{theor.}) + 0.013(m_c - 1.5\ \text{GeV})$, derived from the ratio of Neutral Current (NC) to Charged Current (CC) neutrino iron interaction rates, $R_\nu = \sigma^{NC}/\sigma^{CC} = 0.3072 \pm 0.0025(\text{stat.}) \pm 0.0020(\text{syst.})$ has already been published [1]. An updated value of $\sin^2\theta_W = 0.228$ is given here, the change being due to a different choice (a) for the m_t value (60 instead of 45 GeV) and (b) for the radiative correction program.

A precise measurement of R_ν is important for several reasons:

(a) It allows a precise determination of the electroweak mixing angle $\sin^2\theta_W$.

(b) A comparison of this measurement with the measurement of the boson masses m_Z and m_W provides a stringent test of the Standard Electroweak Model and gives insight into electroweak radiative effects.

(c) A combined analysis of R_ν and $R_{\bar{\nu}}$ determines $\sin^2\theta_W$ and the ρ parameter defined as $\rho = m_W^2/m_Z^2 \cos^2\theta_W$ [2].

(d) One obtains from R_ν and $R_{\bar{\nu}}$ the ratio m_W/m_Z largely independent of $\sin^2\theta_W$.

(e) A precise value of $\sin^2\theta_W$ might also constrain grand unification models.

This precise measurement of $\sin^2\theta_W$ was made possible by progress made both on the experimental and the theoretical side.

The higher experimental accuracy in R_ν compared to the previous experiment [3] could be achieved because of improvements in the experimental technique. The major source of systematic error had previously been due to the so-called Wide Band Beam (WBB) background events. These events are induced by the unknown neutrino flux from unfocused parent particles contributing to the well defined Narrow Band Beam (NBB) neutrino flux. The corresponding uncertainty became insignificant by measuring the WBB background rate. In addition, the beam efficiency was increased giving higher statistical accuracy. Furthermore, a detector upgrade improved the resolution in the transverse event position, making better use of the known dichromatic spectrum of the NBB.

The higher precision in the interpretation of R_ν in terms of electroweak parameters could be achieved by theoretical progress. It was shown by Llewellyn Smith [4] that in an isoscalar target with only massless u and d quarks the largest contributions to the NC and CC cross sections are related by isospin invariance alone. The relation between R_ν and $\sin^2\theta_W$ turns out to be:

$$R_{\nu(\bar{\nu})} = 1/2 - \sin^2\theta_W + 5/9 \sin^4\theta_W (1 + r^{(-1)}) , \qquad (1)$$

Insufficiently known details in describing the real nuclear target are absorbed in the measured CC cross section ratio $r = \sigma_{\bar{\nu}}^{CC}/\sigma_{\nu}^{CC}$. The Quark Parton Model (QPM) with Quantum Chromo Dynamical (QCD) modifications, which in previous analyses was used to relate R_ν to $\sin^2\theta_W$, is now only necessary for small corrections. The outstanding problem left in these corrections is the poor knowledge of the mass of the charmed quark, m_c, which appears as a separate term in the result for $\sin^2\theta_W$.

The main objective of the experiment was to extract $\sin^2\theta_W$ to a precision of ± 0.005 from the measured ratios $R_\nu = N_\nu^{NC}/N_\nu^{CC}$ and $r = N_{\bar{\nu}}^{CC}/N_\nu^{CC}$ in deep inelastic neutrino interactions.

The constants N_ν^{NC}, N_ν^{CC} are the numbers of NC and CC interactions for hadronic energies(*) E_h greater than 10 GeV observed in a neutrino beam and $N_{\bar{\nu}}^{CC}$ is the number of CC interactions in an antineutrino beam having the same energy spectrum as the neutrino beam. The relation (1) between R_ν, $R_{\bar{\nu}}$ r and $\sin^2\theta_W$ shows that: (a) R_ν is about 6 times more sensitive to $\sin^2\theta_W$ than $R_{\bar{\nu}}$ at $\sin^2\theta_W$ values near 0.23; (b) $\Delta\sin^2\theta_W = \pm 0.005$ requires $\Delta R_\nu = \pm 0.003$ (1%); (c) $\Delta r = 0.01$ (2.5% of $r \sim 0.4$) renders the corresponding uncertainty in $\sin^2\theta_W$ negligible. Hence most of the experiment was performed with neutrinos and only about 20% with antineutrinos.

(*) The energy in the laboratory system transferred to the hadronic system in the neutrino interaction.

As in earlier experiments [3,5,6] NC and CC events were separated by their event length: CC events (ν ($\bar{\nu}$) + N $\rightarrow$ μ^- (μ^+) + ...) with a penetrating muon in the final state are long, whereas NC events (ν ($\bar{\nu}$) + N $\rightarrow$ ν (ν) + ...) with only readily absorbed hadrons in the final state are short. Examples of a CC and a NC candidate are shown in fig. 1. The main experimental problem was to correct the NC sample for high-y (= E_h/E_ν) CC events in which the low momentum muon is hidden in the hadron shower (sect. 2.4). In order to minimize systematic uncertainties in the measurement of R_ν and $R_{\bar{\nu}}$, NC and CC events were treated identically throughout the data acquisition and analysis chain. In particular, muon track reconstruction was not used in the analysis. The cut $E_h > 10$ GeV was applied in order to ensure 100% trigger efficiency.

A second objective was to measure the right-handed coupling, g_R^2, of quarks, independently of the R_ν, $R_{\bar{\nu}}$ values, from the difference of the y distributions in NC and CC interactions. This was done by comparing the E_h distribution of NC and CC events as a function of their distance from the beam and using the known correlation between direction and energy of the neutrino in the narrow band beam. A first analysis of this kind had been performed by the CDHS collaboration previously [7].

The layout of the paper is as follows. Sect. 2 describes details about the 1984 experiment with emphasis on the improvements on the beam and the detector compared to previous experiments. The data taking, the selection of NC and CC event samples and the corrections applied thereto are described in this section. Experimental results are given in the form of R_ν, $R_{\bar{\nu}}$, r and hadronic energy distributions in several radial bins for NC and CC events. In sect. 3, the experimental numbers R_ν, $R_{\bar{\nu}}$ and r are first corrected to correspond to the conditions under which relation (1) is valid. Then, $\sin^2\theta_W$ is obtained from R_ν. A combined analysis of R_ν and $R_{\bar{\nu}}$ yields ρ and $\sin^2\theta_W$, m_W/m_Z, and $g^2_{R,L}$. The coupling ratio g_R^2/g_L^2 is also obtained from the difference of the y distributions of NC and CC events. Finally, the results are compared with those obtained from direct measurements of m_W and m_Z. Sect. 4 represents a summary and an outlook.

2. THE EXPERIMENT

2.1 The experimental set-up

2.1.1. The beam

The experiment was performed in 1984 in the CERN NBB facility using 450 GeV protons from the Super Proton Synchroton (SPS). Fig. 2(a) shows the layout of the beam line.

The proton target was a 50 cm long carbon rod with 3 cm diameter. The neutrino parents (π, K) were sign and momentum selected in a 117 m long beam transport system followed by a 292 m long evacuated decay tunnel and a 360 m long shielding arrangement.

The beam optics had been modified with respect to the previous experiments to achieve a higher neutrino event rate per proton on target. An optimum was found [8] by choosing a parent beam energy of 160 GeV and increasing the acceptance of the first group of quadrupoles after the target. As a consequence the momentum bite and divergence increased by 50% to about 14 GeV and 0.4 mrad (FWHM), respectively. The energy spectra of neutrinos and antineutrinos traversing the neutrino detector are shown in fig. 3.

The beam line was instrumented with several monitoring devices which were recorded burst by burst. The intensity of the primary proton beam was measured with a Beam Current Transformer (BCT). Its width and impact point was measured with segmented secondary emission chambers. The absolute intensity of the secondary hadron beam was measured with two other BCT's located a few meters upstream of the decay tunnel as shown in fig. 2(b). A movable set of segmented ionisation chambers installed immediately upstream of the BCT's was used to measure the position and profile of the hadron beam. The composition of the beam was determined with a differential Cherenkov counter moved into the beam in special runs. Eight ionization chambers around the beam pipe upstream of the BCT's served as beam halo monitors. The muon flux was sampled with solid state detectors at various radii and depths in the shielding. Details about the flux measurements can be found in ref. [9]. The time distribution of the beam within a pulse was measured with a scintillator at large shielding depth recording single muons.

Special care was taken to minimize the effect of the badly calculable flux of the so-called Wide Band Beam (WBB) neutrinos from unfocused hadrons. Such neutrinos originate from the decay of hadrons (pions, kaons, charmed particles, ...) produced:

(a) in the proton target and decaying before momentum selection;
(b) anywhere in the beam transport system;
(c) in the decay tunnel in hadron air collisions;
(d) at the beginning of the shielding in hadron Fe collisions.

Source (a) was reduced (as previously) by pointing the proton beam away from the neutrino detector (by 11 mrad horizontally and vertically). Source (b) was reduced by extending the vacuum pipe up to the entrance window of the decay tunnel - only interrupted by a helium filled pipe at the place of the Cherenkov counter. The amount of hadrons produced in the helium and the two additional 10 μm thick Ti windows of this pipe was less than in the equivalent length of air (much less than in the Cherenkov counter) and estimated to be negligible. Source (c) was reduced to a negligible amount by evacuating the decay tunnel to 0.15 Torr. Using results of beam dump experiments [10] source (d) was estimated to be also negligible ($< 10^{-3}$ of the useful flux). The ν flux from sources (a) and (b) was measured by the neutrino event rate obtained in special runs where a 1.5 m long Fe dump at the beginning of the decay tunnel (see fig. 1(b)) was moved into the beam reducing the useful flux to $< 3 \cdot 10^{-4}$ of its normal intensity. This residual flux from the dump was also partially compensated for by source (d). The BCT's guaranteed relative normalisation between runs with and without the dump to better than 0.5%. The NBB flux obtained in this procedure is the flux from hadron decays between the dump position and the end of the decay tunnel.

2.2.2. The Neutrino Detector

The CDHS detector [11] shown in fig. 4(a) was a ~ 22 m long, 1150 t heavy calorimeter consisting of toroidally magnetized iron plates (3.75 m diameter) sandwiched with planes of scintillators (3.6 × 3.6 m^2). The plates were grouped into 21 modules the first 10 of which represent the upgrade of the detector. They consisted of twenty 2.5 cm thick Fe and 0.5 cm thick scintillator plates. The scintillators were split in 24

strips of 15 cm width; each strip was cut in half. Five consecutive half-strips were viewed by a single photomultiplier forming one read-out plane. The strips in consecutive read-out planes were orthogonally oriented (see fig. 4(b)). Thus each of the first 10 modules had 4 read-out planes of 12.5 cm sampling width in the beam direction and 15 cm sampling width in both orthogonal directions perpendicular to the beam. This leads to a transverse spatial resolution of about 5 cm. The signals of opposite photomultipliers were summed; 90% of the sum was fed into Analog-to-Digital Converters (ADC's), 10% being used for triggering.

Modules 11 to 15 each had 15 Fe plates, 5 cm thick and modules 16 to 21 each had five 15 cm thick Fe plates. The 75 scintillator planes in these modules were split in 8 horizontal strips of 47 cm width with the lateral event position being measured by the difference between the signals recorded on each side.

Each of the 21 modules had a central hole for the copper coil producing a toroidal magnetic field of 1.6 Tesla.

Hexagonal drift chambers with three wire planes each (one with horizontal wires, two with wires at ± 30° with respect to the vertical) were in the 31 cm wide gaps in between the modules.

In front of the first module was a 4 x 4 m^2 plane of scintillator sheets (the anticounter) to veto any incoming charged particle produced upstream of the detector.

2.2 Data taking

Data were taken from March to August 1984 with $4.9 \cdot 10^{18}$ protons used for neutrinos and $1.3 \cdot 10^{18}$ protons for antineutrinos. The proton beam was operated in the "fast-slow" extraction mode with 14.4 s repetition time and a nearly gaussian spill shape of ~ 300 μs width at half maximum. At regular intervals the dump was moved into the beam. For statistically optimum WBB background subtraction 28% (37%) of the neutrino (antineutrino) running time was used in this mode.

Data were recorded during a beam gate of 2 ms centered around the beam spill, during a second gate of 2 ms - the so called cosmic gate - for

cosmic ray interactions with identical detector conditions and during a ~ 10 s long gate in between beam pulses - the calibration gate - with a dedicated trigger on nearly horizontal cosmic muons, to calibrate permanently the scintillator and ADC responses.

The data acquisition electronics was triggered by two independent conditions: either if energy was deposited in one (or 2 adjacent) module(s) above a certain threshold (the so called shower trigger) or if a (minimum ionizing) particle penetrated at least 3 modules (the so-called muon trigger). The shower trigger, working identically for NC and CC events, was the trigger used for the R_ν measurement. The muon trigger was used to determine the shower trigger efficiency by observing the shower trigger efficiency for events with a penetrating charged particle and a hadronic shower. Fig. 5 shows the result of this study: Above 10 GeV shower energy the shower trigger efficiency was better than 99.9%.

The detector was busy during ~ 200 ns for an anticounter veto, ~ 160 ns for trigger decision and up to ~ 4 μs for the ADC's after an accepted trigger. The event rates lost during this dead time were different for different run conditions (ν, $\bar{\nu}$, dump out, dump in the beam, cosmics). They had to be measured accurately to minimise the uncertainty in R_ν due to background subtraction. This was done by folding the detector's busy signal distributions with the time distributions of the following signals:

(a) in the beam gate with the time distribution of (i) single muon signals recorded deep in the shielding, (ii) the integral muon flux recorded further upstream in the shielding.

(b) in the cosmic gate with the time distribution of a constant clock.

Comparable deadtimes measured with several methods agreed to within ± 3% of their values. The average deadtime losses were 16.8 ± 1% (7.7 ± 1%) during neutrino (antineutrino) runs without the dump, 12.7 ± 1% (7.4% ± 1%) with the dump in the beam and between 2 and 5% for cosmics.

2.3 Event reconstruction

For each event the hadronic energy, E_h, the event length, L, and the radial distance from the beam axis, R_{beam}, were reconstructed.

2.3.1. Hadron energy measurement

A shower was defined as a cluster of scintillators with more than ~ 6 GeV recorded in a box of 1.5 m Fe length and 1.2 m width, called the shower box. The event vertex was defined by the first read-out plane with a pulse height larger than 1.2 minimum ionizing particles (M.I.P.'s). A second plane hit was required for a valid shower. The hadron energy was measured from the weighted sum of scintillator pulse height recorded in the shower box with its upstream face centered around the event vertex. The weighting was done such that relatively large pulse heights contributed less thus equalizing electromagnetically and hadronically induced signals. The weighting coefficients and the absolute calibration of the calorimeter had been determined from exposures of a few modules to electron and pion beams of known energy [12]. The intrinsic resolution found from these exposures was $\sigma/E = 0.52/\sqrt{E}$ for hadrons, $0.25\ \sqrt{E}$ for electrons.

In NC events the energy recorded in the shower box, E_{sho}, equals the hadron energy, E_h. In CC events E_{sho} contains also the energy E_μ^B deposited by the muon in the shower box. The energy E_μ^B was measured in events with well reconstructed muons from the distribution of the energy deposited in scintillators outside the shower box as a function of the muon momentum p_μ. Fig. 6 shows satisfactory agreement between the mean energy loss thus measured and the one obtained from a simulated muon sample where recent energy loss measurements [15] were used. The effective muon energy loss to be subtracted from E_{sho} was determined such that the number of events above the $E_h > 10$ GeV cut was correct. It was found to be in-between the peak and mean energy loss. The uncertainty in the effective E_h due to this subtraction procedure was ± 150 MeV.

During the analysis it was observed that in the new calorimeter modules the signal height decreased with increasing event rate. This effect could be traced back to an instability of the ADC's and was corrected in the off-line analysis channel by channel using laboratory test results. With a cut on the time lapse of > 10 μs between consecutive events this correction amounted to 5% on the average hadronic energy measurements. It affects NC and CC events equally.

The effective hadronic energy scale and resolution were determined from the data themselves. This was done by comparing at given radii the distribution of the - mainly hadronic - energy of high-y events with that of the - mainly muon - energy of low-y events. From this cross calibration between hadron calorimeter and muon spectrometer, the effective E_h resolution was found to be $\sigma/E_h = 0.6/\sqrt{E_h} + 0.02$. The absolute energy calibration uncertainty was ± 2%.

2.3.2. Event length measurement

The event length L was defined as the thickness of iron parallel to the detector axis between the read-out plane containing the vertex and the last read-out plane hit by the most penetrating particle of the event.

The vertex plane was defined by the shower finding algorithm as the first plane having a pulse height larger than $S_o \hat{=} 1.2$ MIP's. However, the true vertex plane could be different from this first plane due to noise, inefficiencies and back scattered particles. This question was studied by plotting the distance D between the plane containing the shower maximum being well above any threshold and the first plane as a function of S_o. The expected linear rise of the shower onset was observed only from about 3 MIP's onward (fig. 7). The deviation from linearity below 3 MIP's was interpreted as being due to the above mentioned effects. By linear extrapolation to the pulse heights of 0.4 MIP's in modules 1 to 10, 2 MIP's in modules 11-15 corresponding to the minimum number of charged particles in a CC event (two) it was concluded that the true vertex was on average 2 ± 1 cm downstream of the reconstructed one. This was corroborated by finding similar results in both types of modules, which have different scintillator structures.

The search for the last read-out plane of an event was affected by inefficiencies of and noise in the scintillators. A cross-check of the position of the end point is provided by the coarse but reliable measurement using the drift chamber hits (99.96% efficiency, no noise). The average distance between the last scintillator hit and the last drift chamber hit in the data and in a Monte-Carlo simulation sample agreed to within better than 1 cm. Combining the uncertainties of the vertex position and of the end of the event, the measured event length is estimated to be correct on average to better than ± 1.5 cm.

2.4 The NC and CC samples

2.4.1. Event selection

Data taken under bad beam conditions (beam information missing, proton intensity less than 5.10^{12} per pulse) and with malfunctioning detectors were excluded. Events were retained if they fulfilled the following conditions:

- They had occurred inside the beam gate within ± 0.6 ms around the spill centre. This reduced the cosmic ray interaction rate subtraction. Inside the cosmics gate they had to be 25 μs away from the edges of the gate. This excluded unstable detector conditions.
- The time lapse to the preceding event was more than 10 μs thus minimising background, inefficiencies and the E_h correction due to ADC instabilities. This cut excluded 15% (6%) of the neutrino (antineutrino) data during normal run condition (dump out).
- The vertex had to be between the middle of module 3 and the middle of module 10 (the detector region with best resolution in energy and radial position), within a radius of 1.3 m around the detector axis (for good muon acceptance), and outside an area of 40 x 40 cm^2 around the central hole. This fiducial volume weighed 141 t.
- The shower energy E_{sho} was larger than 10 GeV, to ensure full trigger and software efficiency for recognizing showers and reconstructing the event length.
- The first drift chamber upstream of and within 60 cm to the vertex had no hit. This excluded radiative showers generated by incoming muons or by muons from CC events with no visible hadron shower.

After these cuts all of which except the E_{sho} cut affected NC and CC event rates equally, 211266 (9545) events were left from neutrino (antineutrino) runs.

2.4.2. Preliminary separation of NC and CC events

The event length distribution was used to separate NC and CC events: a cut-off length L_c was defined such that practically all NC events had $L < L_c$, all events with $L > L_c$ were CC events (now with $E_h = E_{sho} - E_\mu^B >$

10 GeV) and the number of CC events with a muon shorter than L_c (the "short CC" events) was minimized. In order to follow roughly the longitudinal shower profile L_c was given a logarithmic dependence on E_{sho}:

$$L_c[m] = 0.75 + 0.38 \ln E_{sho} \text{ (GeV)}.$$

Fig. 8 shows the event distribution as a function of L/L_c. Also shown in fig. 8 is the so-called monitor region of CC events defined by $1.4 < L/L_c < 2.4$ and used to normalise the subtraction of short CC events from the NC sample (sect. 2.5.6.).

The raw numbers of NC and CC candidates (line 1 of table 1) had to be corrected to arrive at the final numbers of NC and CC events. The numbers after each correction and the corresponding R_ν, R_ν^- values are given in table 1.

2.4.3. Cosmic ray event subtraction

Cosmic ray induced events were recorded in the cosmic gate and analysed in the same way as beam induced events. Their rate was corrected for the difference in losses due to deadtime and the time lapse cut of 10 μs. Cosmic ray events contaminate mainly the NC sample. The subtraction of cosmic ray events reduces R_ν by 1.8% and R_ν^- by 10.3% with a systematic error of 0.1% and 0.3%, respectively.

2.4.4. Wide band background subtraction

Event rates due to WBB (anti) neutrinos were measured with the dump in the beam. They were corrected for cosmic ray induced background and their rates were normalised to the same parent hadron flux measured with the BCT's as the normal beam taking into account the difference in dead time losses. The event numbers to be subtracted are in line 6 of table 1. Uncertainties in this correction which could be due to incomplete parent beam absorption in the dump, deadtime error, normalisation error etc. were estimated to be less than 4%. It should be noted that this correction (4.3% in the ν beam) caused less than 0.1% uncertainty in R_ν, whereas it was the major cause of uncertainty in the previous experiment without the beam dump facility.

2.4.5. The "long shower" correction

Before subtracting the short CC events from the NC candidates by extrapolating the monitor region into the NC region (see fig. 8), the CC region had to be corrected for a small contamination of NC and short CC events in which the hadron shower was longer than L_c. There were two reasons for this contamination: (a) muons from hadron decays inside the shower; (b) hadron punch-through and/or noise in the scintillators at the end of an event.

The background of events with a muon from hadron decays was estimated from a Monte Carlo simulation of shower development including π, K decay [14] and production and decay of single charmed particles. The result for the neutrino data was that $2.3 \cdot 10^{-3}$ of the events in the NC region migrated into the CC region nearly half of them being true dimuon events (charmed particle decays in short CC events). This could in fact be verified by finding in the monitor region of the neutrino sample 62 ± 17 events with a positive muon compared to 53 ± 16 predicted by the Monte Carlo simulation.

The rate of events with a long shower of the second kind is estimated from the comparison of the event length distribution observed in the data and the one obtained in a Monte Carlo simulation of CC events in which only the propagation of the final state muon in the detector is performed. Fig. 9 shows that this spill-over affected only the region between L_c and the monitor region and amounted to $(1.4 \pm 0.8) \cdot 10^{-3}$ of the NC candidates.

To account for these two effects and avoiding double counting, the long shower correction was combined to be $(2.8 \pm 1.4) \cdot 10^{-3}$ of the NC sample in neutrino runs and $(3 \pm 3) \cdot 10^{-3}$ in antineutrino runs raising R_ν and $R_{-\nu}$ by 0.4 ± 0.2% and 0.4 ± 0.4%, respectively (line 8 and 9 in table 1).

2.4.6. Correction for short CC events

The largest correction was the subtraction of short CC events with $E_{sho} > 10$ GeV from the NC candidates, and the corresponding addition of short CC events with $E_h > 10$ GeV to the CC candidates. This was done by calculating the ratio of the number of short CC events (with $L < L_c$) to

the number of CC events in the monitor region (with 1.4 L_c < L < 2.4 L_c) once for E_{sho} > 10 GeV (f_{sho}, to be applied in the NC region) and once for E_h > 10 GeV (f_h, to be applied in the CC region). The calculation was done with a Monte Carlo simulation describing beam, detector and nucleon structure functions [15] in a QCD improved QPM. The results for f_{sho} and f_h were 0.980 and 0.994 in the neutrino beam, 0.81 and 0.84 in the antineutrino beam, respectively, leading to rather large corrections: 17% of the events in the NC region were short CC events (table 1, line 10). However, the uncertainty in these corrections were relatively small, the largest one being due to a possible bias of ± 1.5 cm in the event length determination (table 2).

CC events could be short because their muon left the detector at the side long before being ranged out or because they were high-y events with a muon range < L_c.

In the first case the uncertainty came from insufficient knowledge of the beam parameters. This has little effect on the correction (table 2), since the focussing magnetic field and the radius cut of 1.3 m (compared to the detector radius of 1.875 m) kept the number of events of this type small (~ 7% of the short CC events). The radial event distribution was well simulated by the Monte Carlo program as shown in fig. 10 for the events in the monitor region.

In the second case - the high-y events - the extrapolation factors depended upon a correct description of the y-distribution of CC events. This dependence is weak, since the monitor region was already a sample of relatively high-y events, with <y> = 0.85 compared to <y> = 0.94 in the NC region. The extrapolation is largely insensitive to uncertainties about beam parameters, detector response and physics assumptions in the Monte Carlo simulation, which reproduced well the observed E_{sho} distribution as shown in fig. 11 for the monitor region. It should be pointed out that this extrapolation did not rely on the shape of the event length distribution below L_c and hence did not need any simulation of the hadron shower details. The main sources of error - apart from a possible bias in the event length - were on the detector side the muon momentum-range relation and on the theoretical side the longitudinal structure function (0.6%). The uncertainty from the momentum range relation of 0.4% accounts for possible multiplicative errors in the magnetic field or momentum loss

along the muon trajectory. The longitudinal structure function defined [16] as the deviation at finite Q^2 from the Callan-Gross relation [17]

$$q_L(x,Q^2) = F_2(x,Q^2) - 2 \times F_1(x,Q^2) \qquad (2)$$

represents a term proportional to (1-y) in the differential cross sections. The uncertainty due to q_L of 0.6% was determined by varying q_L within the limits allowed by the observed y-distribution in CC events shown in fig. 12.

A summary of all uncertainties in the correction for short CC events is given in table 2.

2.4.7 Correction for electron neutrino interactions

The numbers on line 11 of table 1 must finally be corrected for CC events produced by electron neutrinos (ν_e). All ν_e induced events were in the NC candidate sample since the final state electron of the CC ν_e events is hidden in the hadron shower. For these events the measured energy E_{sho} is equal to the neutrino energy E_ν. The ν_e component in the NBB comes entirely from K_{e3} decay and is well calculable. The contribution of ν_e's from the decay of muons in the decay tunnel was estimated to be negligible. The $CC\nu_e$ events with $E_\nu > 10$ GeV had to be subtracted from the NC sample and those with $E_h > 10$ GeV had to be added to the CC sample. This was done by calculating the ratio of the number of $CC\nu_e$ events to the number of $CC\nu_\mu$ events, once for $E_h > 10$ GeV (r_h), and once for $E_\nu > 10$ GeV (r_e) and using the relation

$$R_\nu = \frac{R'_\nu - r_e}{1 + r_h}$$

where the uncorrected ratio R'_ν is taken from line 11 of table 1. The ratios $r_{e,h}$ were calculated by relating the number of $CC\nu_e$ events to the number of CC events induced by neutrinos from $K \to \mu\nu$ decay, the $CC\nu_\mu(K)$ events:

$$r_{e,h} = \frac{CC\nu_e(E_{\nu,h} > 10 \text{ GeV})}{CC\nu_\mu(K) \cdot (1 + R^{\pi/K})}$$

using the Monte Carlo simulation of the experiment. The ratio

$R^{\pi/K} = CC\nu_\mu(\pi)/CC\nu_\mu(K)$ was determined from the radius-versus-energy-plot of the experimental sample of ~ 200 000 $CC\nu_\mu$ events with a reconstructed muon track, in which $CC\nu_\mu(\pi)$ and $CC\nu_\mu(K)$ events are well separated due to the correlation between direction and energy of the neutrinos in a NBB. The $K_{\mu 3}$ decay contribution in the beam and acceptance differences for ν_π and ν_K were accounted for, again using the Monte-Carlo simulation. The results for r_e and r_h were 0.02124 and 0.0175 in the neutrino beam, 0.020 and 0.014 in the antineutrino beam, respectively, leading to the numbers on lines 12 and 13 of table 1. This method of correcting for ν_e events is independent of the K/π ratio as measured with the Cherenkov detector in the beam. The major sources of the systematic uncertainty of 2.5% (3.4%) in the neutrino (antineutrino) case are the K_{e3} branching ratio and the insufficient knowledge of the y-distribution. The latter influences the relation between the event rates for $E_\nu > 10$ and $E_h > 10$ GeV.

2.5 The experimental results

2.5.1. R_ν, $R_{\bar{\nu}}$, r

The final corrected numbers of NC and CC events are given in line 13 of table 1 together with the statistical errors. The systematic errors on R_ν are given in table 3 which summarises the various corrections applied to the NC and CC event samples. Hence the NC to CC cross section ratio for neutrino interactions in iron and for hadronic energy above 10 GeV is

$$R_\nu = 0.3072 \pm 0.0025 \text{ (stat.)} \pm 0.0022 \text{ (syst.)} \qquad (3a)$$

For the antineutrino interactions the systematic uncertainty due to cosmic and WBB background is larger because the event rate is lower and the energy spectrum softer than in the case of neutrino interactions. Also the short CC correction introduces a larger uncertainty due to the poor knowledge of the longitudinal structure function which has a larger effect at high y for antineutrinos than for neutrinos. The final results for antineutrinos is

$$R_{\bar{\nu}} = 0.382 \pm 0.015 \text{ (stat.)} \pm 0.006 \text{ (syst.)}. \qquad (3b)$$

The ratio of CC cross sections for antineutrinos to neutrinos, $r = N_{\bar{\nu}}^{CC}/N_\nu^{CC}$, for $E_h > 10$ GeV, needed to derive $\sin^2\theta_w$ from eq. (1) is obtained from the numbers on line 13 of table 1. It has to be normalised to equal parent hadron fluxes using the BCT's accounting for the different K/π ratios, dead time and time lapse cut losses yielding 0.30 ± 0.01. In

addition it had to be corrected for the difference in the shapes of neutrino and antineutrino spectra. This was done using the Monte-Carlo simulation of the experiment. The result was

$$r = 0.393 \pm 0.005 \text{ (stat.)} \pm 0.013 \text{ (syst.)} . \quad (4)$$

The systematic error arises mainly from uncertainties in the K^-/π^- ratio and the relative BCT normalisation.

In table 4 these results are compared with those of the CHARM experiment [18] performed simultaneously with the experiment described here.

2.5.2. Hadron energy distributions as a function of the beam radius

The total energy E_ν and hence $y = E_h/E_\nu$ for NC events could only be determined via the distance R_{beam} of the events from the beam axis using the energy-radius correlation in the NBB since the energy of the outgoing neutrino could not be reconstructed event by event.

The raw NC and CC event samples were grouped in E_h-R_{beam} bins and the various corrections (for cosmic ray, WBB, short CC and ν_e events) were applied bin by bin. The short CC events were assigned the same E_ν distribution as the CC events in the monitor region to eliminate uncertainties due to the E_h calibration. To account for the different radial distribution of ν_e and ν_μ events and their different composition of electromagnetic and hadronic shower energy a y-dependent correction was applied in the Monte-Carlo program (zero at y = 0 and 1, up to 15% for y = 0.5). Finally, the CC events were used for fine adjustments of the beam parameters. Fig. 13 shows the E_h distribution for NC and CC neutrino and antineutrino events in four radial bins, in good agreement with the Monte-Carlo simulation.

3. DETERMINATION OF THE ELECTROWEAK PARAMETERS

3.1 Correction of R_ν, $R_{\bar{\nu}}$, and r

In the general case of an interaction with only vector and axial vector terms, the largest parts of the NC and CC cross sections are related by isospin invariance alone [4].

At tree level,

$$\frac{d\sigma^{o}_{NC,\nu}}{dy} = g_L^2 \frac{d\sigma^{o}_{CC,\nu}}{dy} + g_R^2 \frac{d\sigma^{o}_{CC,\bar{\nu}}}{dy} + \ldots \quad (5a)$$

$$\frac{d\sigma^{o}_{NC,\bar{\nu}}}{dy} = g_L^2 \frac{d\sigma^{o}_{CC,\bar{\nu}}}{dy} + g_R^2 \frac{d\sigma^{o}_{CC,\bar{\nu}}}{dy} + \ldots \quad (5b)$$

In the Standard Electroweak Model the left and right-handed fermion couplings to the Z are described by

$$g_{Lf} = I_f^3 - Q_f \sin^2\theta_w \quad (6a)$$

$$g_{Rf} = - Q_f \sin^2\theta_w \quad (6b)$$

where I_f^3 and Q_f are the third component of the isospin and the charge of the fermion. Within the QPM, $g_L^2 = g_{Lu}^2 + g_{Ld}^2$ and $g_R^2 = g_{Ru}^2 + g_{Rd}^2$.

The additional terms in eqs (5) describing possible isospin breaking dynamical effects due to strong interactions (higher twist effects), are believed to be small [4], especially in the kinematic range selected by the cut $E_h > 10$ GeV.

Multiplying eqs (5a) and (5b) with the neutrino and antineutrino spectrum (given in fig. 2), respectively, inserting (6) and integrating over the kinematical range of the experiment ($E_h > 10$ GeV) yields the relations

$$R_\nu^o = \frac{1}{2} - \sin^2\theta_w + \frac{5}{9} \sin^4\theta_w (1 + r^o) \quad (7a)$$

$$R_{\bar{\nu}}^o = \frac{1}{2} - \sin^2\theta_w + \frac{5}{9} \sin^4\theta_w \left(1 + \frac{1}{\bar{r}^o}\right), \quad (7b)$$

where r^o ($\bar{r}^o$) is the ratio of $CC\bar{\nu}$ to $CC\nu$ interaction rates with the energy spectrum corrected to take into account the difference between the neutrino and the antineutrinos energy distributions.

In order to extract the ideal quantities R_ν^o, $R_{\bar{\nu}}^o$, r^o, $\bar{r}^o$, from the experimental values R_ν, $R_{\bar{\nu}}$ (3) and r (4), the small non-isoscalarity of the iron nucleus (7% neutron excess), the presence of strange and charmed quarks in the nucleon, threshold effects of the charmed quark mass and radiative effects have to be corrected for.

This has been done with a QCD improved QPM using parametrisations of the quark distribution functions obtained from earlier CC structure function measurements [15]. The mixing between the quark generations has been accounted for by a unitary 3 × 3 Kobayashi Maskawa (KM) matrix with the mixing parameter from ref. [19]. The one-loop radiative corrections have been computed using Bardin's programs [20] for m_t = 60 and m_H = 100 GeV.

The results of the corrections are:

$$\begin{aligned} R_\nu^o &= 0.3122 \pm 0.0034\ (\text{exp.}) - 0.009\ (m_c - 1.5) \\ r^o &= 0.383 \pm 0.014\ (\text{exp.}) + 0.004\ (m_c - 1.5) \end{aligned} \tag{8a}$$

$$\begin{aligned} R_{\bar\nu}^o &= 0.378 \pm 0.016\ (\text{exp.}) - 0.019\ (m_c - 1.5) \\ \bar r^o &= 0.371 \pm 0.014\ (\text{exp.}) + 0.004\ (m_c - 1.5) \end{aligned} \tag{8b}$$

The various corrections and the related uncertainties are given separately in table 5. The correlations between the R_ν and $R_{\bar\nu}$ corrections are displayed in fig. 14, when the QCD improved QPM is used alone (fig. 14(a)) and when it is used together with the Llewellyn-Smith formulae (fig. 14(b)).

The uncertainties due to the poor knowledge of the longitudinal structure function, eq. (2), and due to the normalisation of the sea quark distributions are reduced if the Llewellyn-Smith formulae are used.

The largest uncertainty is due to m_c and its suppression of charm production near threshold in the CC processes

$$\begin{aligned} \nu_\mu + d &\to \mu^- + c, \\ \nu_\mu + s &\to \mu^- + c, \\ \bar\nu_\mu + \bar s &\to \mu^+ + \bar c\ . \end{aligned}$$

The so-called slow rescaling model [21] has been used to account for threshold effects. It assumes free target and charmed quarks - an approximation which may be incorrect around the threshold. The value of

$m_c = 1.5 \pm 0.3$ GeV/c^2 was chosen to reproduce the features of the opposite-sign di-muon data of an earlier CDHS experiment [22] and should be understood as an effective parameter, its error covering both the experimental and theoretical uncertainty. The kinematical suppression of charm production has two effects: (i) it decreases the CC cross section and (ii) it introduces an uncertainty in the NC cross section via the normalisation of the strange sea determined from the antineutrino dimuon data ($\Delta s/s = 0.31\ (m_c - 1.5)$). The correlation between the two effects is accounted for.

An upper bound on the charmed sea distribution has been derived from deep inelastic muon scattering [23]; it is a negligible source of uncertainty.

Also the uncertainty coming from a unitary KM matrix is small. It should be noted that eqs (7) hold also with s and c quarks in the nucleon provided they are massless and have equal distributions. The KM matrix introduces a correction only because isospin symmetry is broken for the s-c doublet ($C \neq S$ and $m_c \neq m_s$). A KM matrix not constrained by unitarity introduces an uncertainty on R_ν of 1.5%. However, even a fourth generation is not expected to shift R_ν significantly because of the quasi-diagonal nature of the KM matrix [4].

The muon mass causes a small correction due to kinematical suppression of the CC process. Terms proportional to m_μ^2 in the CC cross section have been neglected.

Radiative effects cause relatively large corrections: 1.8% on R_ν, 2.5% on R_ν^-. They are of two types, both calculated to first order:

(a) Photonic effects, where a real or virtual photon is emitted by a fermion. These QED effects can be calculated independently of electroweak parameters. The dominant contribution to this large correction (2.3% on R_ν, 2.6% on R_ν^-) comes from photon emission by the muon in the CC process, which has no counterpart in the NC process.

(b) Effects described by electroweak propagators and purely weak box and vertex diagrams. Loop corrections to propagator effects lead to a Q^2 evolution of electroweak coupling constants. Purely weak box

and vertex diagrams modify the neutrino-nucleon cross section calculation. Electroweak corrections depend on the unknown masses m_t and m_H. These masses are treated as free parameters.

The results of the calculation of radiative effects agree with those obtained by various other authors [24-26] within ± 0.002, which is the error assigned to this correction.

3.2 The electroweak parameters

3.2.1 Theoretical framework

At tree level, the definitions of $\sin^2\theta_W$ via the electroweak coupling constants, $\sin^2\theta_W = e^2/g^2$ and via the boson masses, $\sin^2\theta_W = 1 - m_W^2/m_Z^2$, coincide. As soon as electroweak radiative effects are considered, the definitions differ slightly, thereby introducing a conceptual problem as to the meaning of $\sin^2\theta_W$. The present experimental accuracy is such that the problem cannot be ignored.

In the absence of a universally accepted definition, the one that seems to be today most widely used is adopted [27]: $\sin^2\theta_W \equiv 1 - m_W^2/m_Z^2$.

Below, an analysis of the experimental results is presented in terms of the Standard Electroweak Model, with $\rho = 1$. The results are also analysed in terms of an extension of the Standard Electroweak Model, with ρ and $\sin^2\theta_W \equiv 1 - m_W^2/\rho m_Z^2$ as free parameters.

3.2.2. $\sin^2\theta_W$ from R_ν

Using the experimental values (3) and (4) for R_ν and r, eq. (7a) would yield $\sin^2\theta_W = 0.236$. With the corrected values (8a), R^o and r^o, eq. (7a) yields (m_t = 60 GeV, m_H = 100 GeV and $\rho = 1$):

$$\sin^2\theta_W = 1-m_W^2/m_Z^2 = 0.228 \pm 0.005 \text{ (exp.)} \pm 0.003 \text{ (theor.)} + 0.013\ (m_c - 1.5)$$

or with the error assigned to m_c (± 0.3 GeV/c^2):

$$\sin^2\theta_W = 0.228 \pm 0.005 \text{ (exp.)} \pm 0.005 \text{ (theor.)}.$$

The experimental error results from the statistical and systematic errors on R_ν and r, added in quadrature. In the last column of table 5 and in fig. 15 the effect of each R_ν correction on $\sin^2\theta_W$ as well as its uncertainty is displayed. The difference between the present and the previously published value $\sin^2\theta_W = 0.225$ [1] is due to the smaller radiative correction obtained with Bardin's programs ($\Delta\sin^2\theta_W = + 0.002$) and due to a different reference value for m_t (60 GeV instead of 45 GeV, $\Delta\sin^2\theta_W = + 0.001$). The dependence of $\sin^2\theta_W$ on m_t and m_H is given in fig. 16. It is rather weak considering the experimental error.

3.2.3. m_t limit from R_ν and $R_{\bar{\nu}}$

For a more precise analysis of $R_{\bar{\nu}}$, the results of the present experiment have been combined with those obtained from an earlier exposure [3] in a 200 GeV NBB: $R_{\bar{\nu}} = 0.363 \pm 0.015$. This number has been adjusted to the conditions of the present experiment, and a weighted average of 0.375 ± 0.011 is used in the following.

For a given value of $\sin^2\theta_W = 1 - m_W^2/m_Z^2$, the prediction of the Standard Electroweak Model for R_ν and $R_{\bar{\nu}}$ depends on m_t and m_H as shown in fig. 17. For fortuitous numerical reasons R_ν is sensitive to $\sin^2\theta_W$, while $R_{\bar{\nu}}$ is particularly sensitive to m_t. From this analysis an upper limit for the top quark mass is obtained (for $\rho = 1$):

$$m_t < 240 \text{ GeV (90\% c.l.)}.$$

The sensitivity to m_H is insignificant at this level of precision.

3.2.4. ρ and $\sin^2\theta_W$ from R_ν and $R_{\bar{\nu}}$

In an extended Standard Electroweak Model eqs (7) are written as functions of ρ and $\sin^2\theta_W = 1 - m_W^2/(\rho m_Z^2)$:

$$R_\nu^o = \rho^2 \left(\frac{1}{2} - \sin^2\theta_W + \frac{5}{9} (1 + r^o) \sin^4\theta_W \right) \qquad (9a)$$

$$R_{\bar{\nu}}^o = \rho^2 \left(\frac{1}{2} - \sin^2\theta_W + \frac{5}{9} \left(1 + \frac{1}{\bar{r}^o}\right) \sin^4\theta_W \right) . \qquad (9b)$$

A common fit of the data to eqs (9) yields:

$$\rho = 0.991 \pm 0.020 \text{ (exp.)} - 0.023 \ (m_c - 1.5)$$

$$\sin^2\theta_W = 0.218 \pm 0.021 \text{ (exp.)} - 0.011 \ (m_c - 1.5)$$

for $m_t = 60$ GeV, $m_H = 100$ GeV. These results depend strongly on the choice for m_t.

The theoretical uncertainty on ρ and $\sin^2\theta_W$ is negligible compared to the experimental error. The experimental error on ρ (2%) arises mainly from $R_{\bar{\nu}}$ (4%). Note that the charm threshold effects on $\sin^2\theta_W$ determined from the two and one-parameter fits have opposite sign.

3.2.5. m_W/m_Z from R_ν and $R_{\bar{\nu}}$

Remaining in the extended Standard Electroweak Model, ρ and $\sin^2\theta_W$ can be changed to m_W/m_Z and $\sin^2\theta_W$ as free parameters.

Replacing ρ by $(m_W/m_Z)^2/\cos^2\theta_W$ in eqs (9a)-(9b) yields

$$R_\nu^o = \left(\frac{m_W}{m_Z}\right)^4 \frac{\frac{1}{2} - \sin^2\theta_W + \frac{5}{9}(1 + r^o)\sin^4\theta_W}{(1 - \sin^2 r_W)^2}, \qquad (10a)$$

$$R_{\bar{\nu}}^o = \left(\frac{m_W}{m_Z}\right)^4 \frac{\frac{1}{2} - \sin^2\theta_W + \frac{5}{9}\left(1 + \frac{1}{r^o}\right)\sin^4\theta_W}{(1 - \sin^2\theta_W)^2}. \qquad (10b)$$

Numerically, it turns out that eq. (10a) is a weak function of $\sin^2\theta_W$:

$$R_\nu^o = \frac{1}{2}\left(\frac{m_W}{m_Z}\right)^4 (1 + 0.15 \sin^4\theta_W) :$$

Hence, R_ν represents a measurement of the mass ratio m_W/m_Z largely independent of $\sin^2\theta_W$ and therefore of the values of the ρ parameter, m_t and m_H. A combined fit to R_ν^o and $R_{\bar{\nu}}^o$ yields:
$m_W/m_Z = 0.880 \pm 0.002(\text{exp.}) \pm 0.002 \text{ (theor.)} - 0.007 \ (m_c - 1.5) =$
0.880 ± 0.0035.

3.2.6. Determination of the right- and left-handed couplings

So far the NC-quark couplings are assumed to be described by the formulae eq. (6). However, the Lagrangian leading to eq. (5) is general

enough to account for any QPM with vector and axial vector currents and eqs (5) can be kept in their general form. Eqs (7) become

$$R_\nu^o = g_L^2 + g_R^2 \, r^o \tag{11a}$$

$$R_{\bar{\nu}}^o = g_L^2 + g_R^2 \frac{1}{r^o} \tag{11b}$$

A fit of the data to eq. (11) gives

$$g_L^2 = 0.300 \pm 0.006$$

$$g_R^2 = 0.029 \pm 0.005$$

These values are in good agreement with the predictions of the Standard Electroweak Model for $\sin^2\theta_w = 0.228$, $g_L^2 = 0.300$ and $g_R^2 = 0.029$. The errors include the theoretical errors. Right-handed quark coupling is demonstrated by g_R^2 being close to 6 standard deviations above zero.

The QPM can be used to parametrize R_ν, $R_{\bar{\nu}}$ in terms of the u and d quark couplings separately (assuming identical couplings for equal-charge quarks: $g_{Lc} = g_{Lu}$, $g_{Ls} = g_{Ld}$, ...):

$$R(\bar{\nu}) = (1 - {}^{(\bar{\delta})}) \, (a_{Lu}g_{Lu}^2 + a_{Ld}g_{Ld}^2 + a_{Ru}g_{Ru}^2 + a_{Rd}g_{Rd}^2) \ ,$$

where ${}^{(\bar{\delta})}$ represent the photonic contributions to the radiative corrections. The values for δ and the coefficients $a_{L,R;u,d}$ for this experiment are given in table 6 for $m_c = 1.5$ GeV together with the values for $R_{\bar{\nu}}$ of the 1979 experiment.

3.3 Analysis of the y-distribution of neutral current events

The space time structure of the neutral current can be studied independently by comparing the NC and CC y-distributions. This information is contained in the (E_h, R_{beam}) - distributions given in sect. 2.5.2. and fig. 13. In order to be independent of the normalisation - an information already used to extract g_L^2, g_R^2 from R_ν and $R_{\bar{\nu}}$ - a fit of the ratio g_R^2/g_L^2 to the shapes of the (E_h, R_{beam}) - distributions has been performed. Using neutrino and antineutrino data together yields

$$g_R^2/g_L^2 = 0.11 \pm 0.04 \ (\text{stat.}) \pm 0.04 \ \ (\text{syst.}) \ ,$$

in good agreement with the prediction for $\sin^2\theta_w = 0.228$: $g_R^2/g_L^2 = 0.097$.

In order to display the presence of right-handed coupling in the neutral current graphically the NC/CC ratio as a function of y was extracted from the data. The Monte-Carlo simulation of the experiment was used to relate the (E_h, R_{beam})-bins to y-bins. The ratio of the y-distributions was chosen since it is less sensitive to systematic errors than the y distributions of NC and CC events separately. Fig. 18 shows that the NC/CC ratio falls significantly with y in the neutrino data and rises significantly with y in the antineutrino data.

This analysis allows also a determination of $\sin^2\theta_W$, independently of the value of the ρ parameter:

$$\sin^2\theta_W = 0.24 \pm 0.03 \text{ (stat.)} \pm 0.03 \text{ (syst.)}.$$

3.4 Comparison with electroweak parameters from $p\bar{p}$ results

The masses of the W and Z bosons have been measured in $p\bar{p}$ collisions. The published results of the two UA experiments at CERN [28],

$$m_W = 82.7 \pm 1 \text{ (stat.)} \pm 2.7 \text{ (energy scale) GeV and}$$
$$80.2 \pm 0.6 \text{ (stat.)} \pm 0.5 \text{ (syst.)} \pm 1.3 \text{ (energy scale)},$$
$$m_Z = 93.1 \pm 1 \text{ (stat.)} \pm 3.1 \text{ (energy scale) and}$$
$$91.5 \pm 1.2 \text{ (stat.)} \pm 1.7 \text{ (energy scale)}$$

for UA1 and UA2, respectively, yield averages of

$$m_W = 80.7 \pm 1.3 \text{ GeV}, \quad m_Z = 91.9 \pm 1.8 \text{ GeV},$$

and a mass ratio of

$$m_W/m_Z = 0.882 \pm 0.011 \text{ (stat.)}.$$

These values permit two tests of the Standard Electroweak Model.

3.4.1 Relation between R_ν and m_W

From the comparison of $\sin^2\theta_W$ as determined from R_ν (sect. 3.2.2) with $\sin^2\theta_W$ as determined from m_W a measurement of the radiative correction parameter Δr is possible. It is defined by the relation [27]

$$m_W^2 = \frac{\pi\alpha}{\sqrt{2}\, G_\mu} \quad \frac{1}{\sin^2\theta_W} \quad \frac{1}{1-\Delta r} ,$$

where α is the fine structure constant, and G_μ the Fermi coupling constant as measured in muon decay. One finds

$$\Delta r = 0.057 \pm 0.030 \text{ (from } m_W) \pm 0.030 \text{ (from } R_\nu)$$

in agreement with the value $\Delta r = 0.071 \pm 0.0013$ predicted by the Standard Electroweak Model (for $m_t = 60$ GeV, $m_H = 100$ GeV).

The relation between R_ν and m_W depends for a given $\sin^2\theta_W = 1 - m_W^2/m_Z^2$ on m_t (and, albeit insignificantly, on m_H) as shown in fig. 19. It can be interpreted as an upper limit on the top quark mass

$$m_t < 240 \text{ GeV (90\% CL)},$$

which is independent of the one in sect. 3.2.3.

3.4.2 Comparison between the mass ratios

The uncertainties in the $R_\nu - m_W$ comparison due to m_t and m_H are absent in the comparison of the m_W/m_Z ratios from R_ν and $p\bar{p}$ results.

The values m_W/m_Z of 0.880 ± 0.0035 from R_ν and 0.882 ± 0.011 from the mass measurements are in remarkable agreement providing a test of the Standard Electroweak Model at the ~ 1% level. A deviation from this agreement would indicate a breakdown of the $SU(2)_L \times U(1)$ gauge structure. At present the value extracted from neutrino nucleon scattering experiments is more precise than the one from $p\bar{p}$ collision experiments; this test will become more stringent when direct measurements of the mass ratio with higher precision become available. However, it is worth noting, that within the Standard Electroweak Model the present experiment predicts the W mass to better than $\pm$ 320 MeV once m_Z is measured to better than $\pm$ 50 MeV in the near future at SLC and LEP.

4. SUMMARY AND OUTLOOK

The ratios R_ν and $R_{\bar{\nu}}$ of NC to CC neutrino and antineutrino interaction rates have been measured in a high-statistics neutrino-iron scattering

experiment with an improved beam and detector. In the case of R_ν the experimental error matches the theoretical error which is dominated by the uncertainty about the charmed quark mass. The error of $R_{\bar{\nu}}$ is still dominated by statistics.

The results derived from these measurements are:

(a) From R_ν a value for $\sin^2\theta_W \equiv 1 - (m_W/m_Z)^2 = 0.228 \pm 0.005 \pm 0.005$ valid for $m_t = 60$ GeV, $m_H = 100$ GeV, and $\rho = 1$.

(b) From a combined R_ν, $R_{\bar{\nu}}$ analysis the values $\sin^2\theta_W = 1 - [m_W/(\rho\, m_Z)]^2 = 0.218 \pm 0.021$ (exp.) $\pm$ 0.006 (theor.) and $\rho = 0.991 \pm 0.020$ (exp.) $\pm$ 0.009 (theor.), also for $m_t = 60$ GeV, $m_H = 100$ GeV, or - for $\rho = 1$ - an upper limit for the top quark mass, $m_t < 240$ GeV (90% CL).

(c) The R_ν, $R_{\bar{\nu}}$ analysis also yields a precise m_W/m_Z ratio of 0.880 $\pm$ 0.0035, which is valid in $SU(2)_L \times U(1)$ independent of assumptions about m_t and m_H.

(d) An analysis of R_ν, $R_{\bar{\nu}}$ yields values for the left- and right-handed NC coupling constants, $g_L^2 = 0.300 \pm 0.006$, $g_R^2 = 0.029 \pm 0.005$.

(e) The presence of right-handed coupling of the NC is also demonstrated by the difference of NC and CC y distributions.

The value for $\sin^2\theta_W$ agrees well with the one measured by the CHARM experiment [18] in the same beam. Together with the CHARM result, this experiment provides the presently most accurate measurement of the electroweak mixing parameter, $\sin^2\theta_W = 0.232 \pm 0.004 \pm 0.005$. See also ref. [26] for a global analysis of all existing data. Comparing the corresponding mass ratio m_W/w_Z with the one obtained from direct mass measurements in $p\bar{p}$ pp collisions represents a test of the $SU(2)_L \times U(1)$ gauge structure at the 1% level.

The results obtained in νN scattering will remain important ingredients to the theory of electroweak interactions especially when SLC and LEP measure m_Z and Z couplings and when $p\bar{p}$ colliders measure more precisely the m_W/m_Z ratio.

They will also serve to constrain Grand Unified Theories (GUT's) as discussed by many authors [29]. The measured $\sin^2\theta_W$ value lies in the range of predictions by several GUT's, but seems to exclude the minimal non-supersymmetric SU(5) GUT which suggests a smaller value for $\sin^2\theta_W$ (and also a proton lifetime below experimental bounds).

Acknowledgements

It is a pleasure to thank the staff of the CERN Experimental Facilities and Accelerator Divisions for the timely installation of the new NBB line and of its monitoring devices, and for the excellent operation of the accelerator complex. We are grateful to our many technical collaborators from the participating institutes for the construction and maintenance of the detector and for their help with running the experiment. We are indebted to D. Yu. Bardin, L. Maiani, R. Peccei, R. Petronzio, R.G. Stuart and J.F. Wheater for helpful discussions on the theoretical interpretation of the experimental results.

REFERENCES

[1] H. Abramowicz et al., Phys. Rev. Lett. 57 (1986) 298.

[2] (a) D.A. Ross and M. Veltman, Nucl. Phys. B95 (1975) 135;
(b) M. Veltman, Nucl. Phys. B123 (1977) 89;
(c) W.J. Marciano and A. Sirlin, Phys. Rev. D29 (1984) 945;
erratum: Phys. Rev. D31 (1985) 213.

[3] H. Abramowicz et al., Zeitschr. für Phys. C28 (1985) 51.

[4] C.H. Llewellyn-Smith, Nucl. Phys. B228 (1983) 205.

[5] M. Holder et al., Phys. Lett. 71B (1977) 222.

[6] B.C. Barish et al., Phys. Rev. Lett. 34 (1975) 538;
F.S. Merritt et al., Phys. Rev. D17 (1978) 2199.

[7] M. Holder et al., Phys. Lett. 72B (1977) 254.

[8] A. Grant and J.M. Maugain, CERN Internal Report CERN/EF/Beam 83-2.

[9] P. Berge et al., Zeitschr. für Phys. C35 (1987) 443.

[10] H. Grässler et al., Nucl. Phys. B273 (1986) 253;
P. Perez, in Proc. Intern. Europhysics Conf. on High Energy Physics, Brighton (1983) 316.

[11] M. Holder et al., Nucl. Instr. and Meth. 148 (1978) 235.

[12] H. Abramowicz et al., Nucl. Instr. and Meth. 180 (1981) 429.

[13] R. Kopp et al., Zeitschr. für Phys. C28 (1985) 171.

[14] H. Burkhardt et al., Zeitschr. für Phys. C31 (1986) 39.

[15] H. Abramowicz et al., Zeitschr. für Phys. C17 (1982) 283;
H.D. Brummel, Diplomarbeit (unpubl.), University of Dortmund (1984).

[16] G. Altarelli and G. Martinelli, Phys. Lett. 76B (1978) 89.

[17] G.G. Callan and D.J. Gross, Phys. Rev. Lett. 22 (1969) 156.

[18] J.V. Allaby et al., Phys. Lett. 177B (1986) 446;
J.V. Allaby et al., Zeitschr. für Phys. C36 (1987) 611.

[19] K. Kleinknecht and B. Renk, Phys. Lett. 130B (1983) 459.

REFERENCES (Cont'd)

[20] D. Yu. Bardin, P.Ch. Christova and O.M. Fedorenko, Nucl. Phys. B175 (1980) 435;

D. Yu. Bardin, P.Ch. Christova and O.M. Fedorenko, Nucl. Phys. B197 (1982) 1;

D. Yu. Bardin and V.A. Dokuchaeva, Dubna preprint E2-86-260 (1986).

[21] R.M. Barnett, Phys. Rev. D14 (1976) 70;

H. Georgi and H.D. Politzer, Phys. Rev. D14 (1976) 1829.

[22] H. Abramowicz et al., Zeitschr. für Phys. C15 (1982) 19.

[23] J.J. Aubert et al., Nucl. Phys. B213 (1983) 31.

[24] G. Gounaris and D. Schildknecht, Zeitschr. für Phys. Rev. C40 (1988) 447, Zeitschr. für Phys. Rev. C42 (1989) 107.

[25] (a) J.F. Wheater and Ch.H. Llewellyn Smith, Nucl. Phys. B208 (1982) 27; erratum: Nucl. Phys. B226 (1983) 547;

(b) A. Sirlin and W.J. Marciano, Nucl. Phys. B189 (1981) 442;

(c) L. Liede et al., Helsinki University preprint HU-TFP-8345 (1983);

(d) M. Roos, private communication.

[26] U. Amaldi et al., Phys. Rev. D36 (1987) 1385.

[27] A. Sirlin, Phys. Rev. D22 (1980) 971.

[28] C. Albajar et. al., (UA1 Collaboration), CERN/EP 88-168, submitted to Zeitschr. für Phys. C;

R. Ansari et al., (UA2 Collaboration), Phys. Lett. 186B (1987) 440.

[29] G.G. Ross, Grand Unified Theories, Benjamin/Cummings Publishing Company 1984.

Table 1

Corrections of the NC and CC data samples and the corresponding R_ν and $R_{\bar{\nu}}$ values

Line			Neutrino Beam					Antineutrino Beam				
			NC region $E_{sho} > 10$	CC region $E_h > 10$ GeV	R_ν	Monitor region $E_{sho} > 10$	Monitor region $E_h > 10$ GeV	NC region $E_{sho} > 10$	CC region $E_h > 10$ GeV	$R_{\bar{\nu}}$	Monitor region $E_{sho} > 10$	Monitor region $E_h > 10$ GeV
1	Data with normal beam	In beam gate	60936 ± 252	137853 ± 371	0.4420 ± 0.0021	10567 ± 103	10219 ± 101	2967 ± 55	5573 ± 75	0.532 ± 0.012	298 ± 17	261 ± 16
2		In cosmics gate (normalised)	1120 ± 25	9 ± 2		5 ± 2	4 ± 2	312 ± 14	5 ± 2		1 ± 1	1 ± 1
3			59816 ± 253	137844 ± 371	0.4339 ± 0.0021	10562 ± 103	10215 ± 101	2655 ± 57	5568 ± 75	0.477 ± 0.012	297 ± 17	260 ± 16
4	Data with dump in beam	In beam gate	1277 ± 36	1645 ± 41		212 ± 15	183 ± 14	234 ± 15	144 ± 12		30 ± 5	24 ± 5
5		In cosmics gate (normalised)	352 ± 15	2 ± 1		1 ± 1	1 ± 1	112 ± 8	0		1 ± 1	0
6	WBB background events		925 ± 39	1643 ± 41		211 ± 15	182 ± 14	122 ± 17	144 ± 12		29 ± 5	24 ± 5
7	Data corrected for cosmics and WBB		56896 ± 277	132657 ± 393	0.4289 ± 0.0024	9896 ± 113	9640 ± 110	2367 ± 70	5228 ± 80	0.453 ± 0.015	228 ± 21	203 ± 20
8	Long shower correction		+ 159	− 158		− 57	− 57	− 7	− 6		− 2	− 2
9			57055 ± 282	132499 ± 393	0.4306 ± 0.0025	9839 ± 113	9583 ± 110	2374 ± 70	5222 ± 80	0.455 ± 0.015	226 ± 21	201 ± 20
10	Short CC correction		− 9642 ± 111	+ 9526 ± 110				− 183 ± 17	+ 168 ± 16			
11			47413 ± 303	142025 ± 408	0.3338 ± 0.0025			2191 ± 72	5390 ± 85	0.406 ± 0.015		
12	$\nu_e(K_{e3})$ correction		− 3016 ± 56	+ 2488 ± 52				− 103	+ 73			
13	Final samples		44397 ± 308	144513 ± 411	0.3072 ± 0.0025			2088 ± 73	5463 ± 81	0.382 ± 0.015		

Table 2

Systematic errors (in %) on the short CC subtraction

	Source	Error
Beam	NBB energy ± 2 GeV	0.02
	K/π ratio ± 5%	0.08
	position of centre ± 1 cm	0.08
	divergence ± 0.02 mrad	0.10
	Total beam	0.15
Detector	energy calibration	0.10
	energy resolution	0.10
	vertex resolution	0.06
	momentum-range relation	0.40
	event length bias	1.10
	Total detector	1.18
Theory	longitudinal structure function	0.60
	fraction of antiquarks	0.00
	total cross section vs. energy	0.16
	Q^2 evolution	0.05
	radiative corrections	0.10
	Monte-Carlo statistics	0.75
	Total theory	0.98
Total		1.60

Table 3

Effect of event sample corrections on R_ν and $R_{\bar{\nu}}$

Nature of correction	$\frac{\Delta R_\nu}{R_\nu}$ (%)	error (%)	$\frac{\Delta R_{\bar{\nu}}}{R_{\bar{\nu}}}$ (%)	error (%)
Muon energy loss in shower box		0.4		1.2
Cosmic ray event subtraction	- 1.8	0.1	- 10.3	0.3
WBB background subtraction	- 1.2	0.1	- 5.0	0.3
Long showers	+ 0.4	0.2	+ 0.4	0.2
Short CC	- 22.5	0.45	- 10.8	0.6
Electron neutrino events	- 8.0	0.2	- 6.1	0.2
Total systematic error		0.68		1.5

Table 4

Comparison of R_ν, $R_{\bar{\nu}}$, and r-values between this and the CHARM Experiment [20]

	R_ν	$R_{\bar{\nu}}$	r
This experiment	0.3072 ± 0.0033	0.382 ± 0.016	0.393 ± 0.014
Corrected for non-isoscalarity	0.3135 ± 0.0033	0.376 ± 0.016	0.409 ± 0.014
Same, extrap. for $E_h > 4$ GeV	0.3167	0.371	0.453
CHARM, $E_h > 4$ GeV	0.3093 ± 0.0031	0.390 ± 0.014	0.456 ± 0.011
CHARM, $E_h > 9$ GeV	0.3052 ± 0.0033	0.397 ± 0.015	0.429 ± 0.010

Table 5

Corrections and uncertainties on the corrected value for R_ν and $R_{\bar{\nu}}$ (in %), when the QCD improved QPM only is used (QPM) and when the Llewellyn-Smith formulae are used (LS). In the last column the effect on $\sin^2\theta_W$ extracted from R_ν and r is given. The effect of each correction is given with all other corrections applied.

Correction due to:	$\Delta R_\nu/R_\nu$ (%)		$\Delta R_{\bar{\nu}}/R_{\bar{\nu}}$ (%)		$\Delta\sin^2\theta_W$
	QPM	LS	QPM	LS	
μ mass	+ 0.2 –	+ 0.2 –	+ 0.2 –	+ 0.2 –	+ 0.0008 –
Propagator Q^2/M^2	+ 0.1 –	+ 0.1 –	+ 0.0 –	+ 0.03 –	+ 0.0003 –
Unitary KM matrix $\lvert U_{ud}\rvert^2 \pm 0.0024$	+ 0.6 $\mp$ 0.0	+ 0.6 $\mp$ 0.0	+ 0.3 $\mp$ 0.0	+ 0.4 $\mp$ 0.03	+ 0.0030 $\mp$ 0.0001
Non-isoscalarity $U_V/D_V \pm 10\%$	– 2.0 $\overline{+}$ 0.2	– 1.9 $\overline{+}$ 0.2	+ 1.6 $\overline{+}$ 0.16	+ 0.8 $\overline{+}$ 0.08	– 0.0090 $\overline{+}$ 0.0009
Longitudinal structure function $\pm$ 50%	+ 0.3 $\pm$ 0.16	+ 0.1 $\pm$ 0.07	– 1.4 + 0.6	+ 0.1 $\pm$ 0.05	+ 0.0006 $\pm$ 0.0003
Quark sea $(\bar{U} + \bar{D})/(U + D) \pm 20\%$	+ 1.3 $\pm$ 0.2	+ 0.4 $\pm$ 0.07	– 8.6 $\mp$ 1.0	– 1.0 $\mp$ 0.16	+ 0.0020 $\pm$ 0.0003
Strange sea $\bar{S}/\bar{D} \pm 30\%$	+ 1.2 $\pm$ 0.3	+ 1.2 $\pm$ 0.2	+ 0.8 $\pm$ 0.2	+ 1.9 $\pm$ 0.5	+ 0.0046 $\pm$ 0.0010
C/S 0.2 $\pm$ 100%	+ 0.1 $\pm$ 0.1	+ 0.1 $\pm$ 0.1	– 0.03 $\mp$ 0.03	+ 0.13 $\pm$ 0.13	+ 0.0005 $\pm$ 0.0005
Radiative effects	– 1.8 $\pm$ 0.4	– 1.8 $\pm$ 0.4	– 2.5 $\pm$ 0.6	– 2.5 $\pm$ 0.6	– 0.0090 $\pm$ 0.0020
Error from r $\pm$ 0.013	–	$\pm$ 0.1	–	$\pm$ 0.7	$\pm$ 0.0002
Total theoretical error (excluding m_c)	$\pm$ 0.34	$\pm$ 0.24	$\pm$ 1.2	$\pm$ 1.24	$\pm$ 0.003
m_c 1.5 GeV $\pm$ 0.3 GeV	+ 2.4 $\pm$ 0.9	+ 2.3 $\pm$ 0.9	+ 3.1 $\pm$ 1.4	+ 3.9 $\pm$ 1.5	+ 0.0110 $\pm$ 0.0042

Table 6

Correction coefficients which multiply the individual chiral couplings

	δ	a_{Lu}	a_{Ld}	a_{Ru}	a_{Rd}
R_{ν}^{CDHS84}	0.023	0.936	1.045	0.379	0.453
$R_{\bar{\nu}}^{CDHS84}$	0.026	0.948	1.134	2.411	2.690
$R_{\bar{\nu}}^{CDHS79}$	0.024	0.944	1.126	2.295	2.563

FIGURE CAPTIONS

Fig. 1 Computer display of a CC and NC candidate.

Fig. 2 (a) Overall view of the 1984 160 GeV Narrow Band Beam.

(b) Details of the section before the decay tunnel showing the monitors in front of the dump.

Fig. 3 The spectra of (a) ν_μ (solid line) and ν_μ (dashed line) inside the acceptance of the detector after the geometrical cuts and (b) ν_μ from Ke_3 decay.

Fig. 4 (a) Layout of the CDHS detector.

(b) Structure of the new type of CDHS modules.

Fig. 5 The shower trigger efficiency as a function of the shower energy, calculated from CC events recorded by the muon trigger.

Fig. 6 The response of the detector inside a box of 1.5 mm length to isolated muons as a function of their momentum. The full circles correspond to the data, the open circles to the simulated values. The absolute scale of the simulated points is chosen to match the data points in average.

Fig. 7 Thresholds required for the first scintillator versus distance D between the vertex and the shower maximum.

Fig. 8 Distribution of the event length L, in units of the cut-off L_{cut} (see text), for neutrino events with $E_h > 10$ GeV. The background from cosmic rays and WBB has been subtracted.

Fig. 9 The shape of the event length distribution near the cut-off L_{cut} showing a small spill-over of long showers in the CC signal region.

Fig. 10 Radial event distribution in the monitor region.

FIGURE CAPTIONS (Cont'd)

Fig. 11 E_{sho} distribution of events in the monitor region.

Fig. 12 y distribution of the CC events.

Fig. 13 E_h distribution of NC and CC events in 4 radial bins.

Fig. 14 Nucleon structure corrections to R_ν and $R_{\bar{\nu}}$ when (a) the QCD improved QPM is used alone and (b) when it is used together with the Llewellyn-Smith formulae.

Fig. 15 Effect (arrow) of switching off any one correction (but applying all others) and uncertainties (square box) due to the corrections on $\sin^2\theta_W$.

Fig. 16 $\sin^2\theta_W = 1 - (m_W/m_Z)^2$ as extracted from R_ν and r using Bardin's radiative correction programs [24] for three m_H values.

Fig. 17 R_ν versus $R_{\bar{\nu}}$ for various $\sin^2\theta_W$ values as a funtion of m_t. The dotted curve indicates the effect of changing m_H from 100 GeV to 1000 GeV.

Fig. 18 Ratio of NC to CC y distributions for neutrino and antineutrino interactions. The error bars are statistical errors on each point. The full lines are 1 standard deviation contours combining statistical and systematic errors accounting for their large and positive point-to-point correlations; the effect of varying the theoretical parameters within the range of table 4 (including $0.16 < \sin^2\theta_W < 0.30$) are taken into account and radiative effects are corrected for.

Fig. 19 Relation between m_W and R_ν for various m_Z and two ρ values as a function of m_t. The dotted curve indicates the effect of changing m_H from 100 GeV to 1000 GeV.

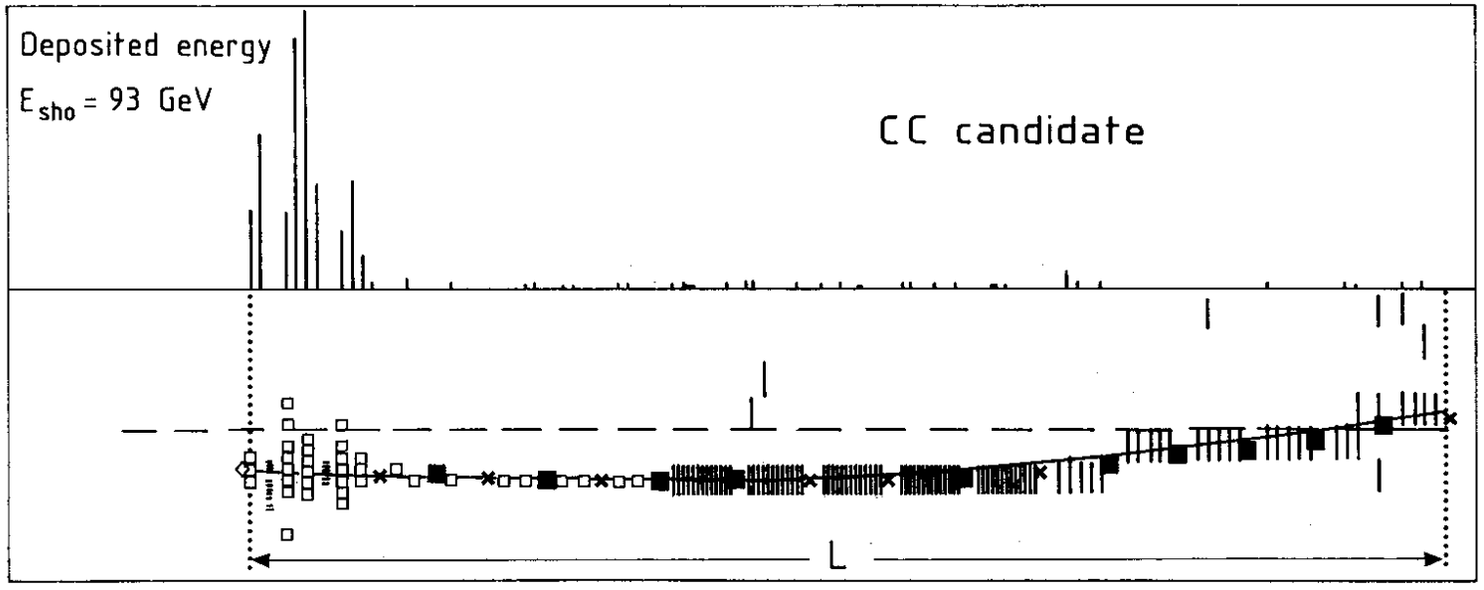
Deposited energy
E_{sho} = 93 GeV
CC candidate
L

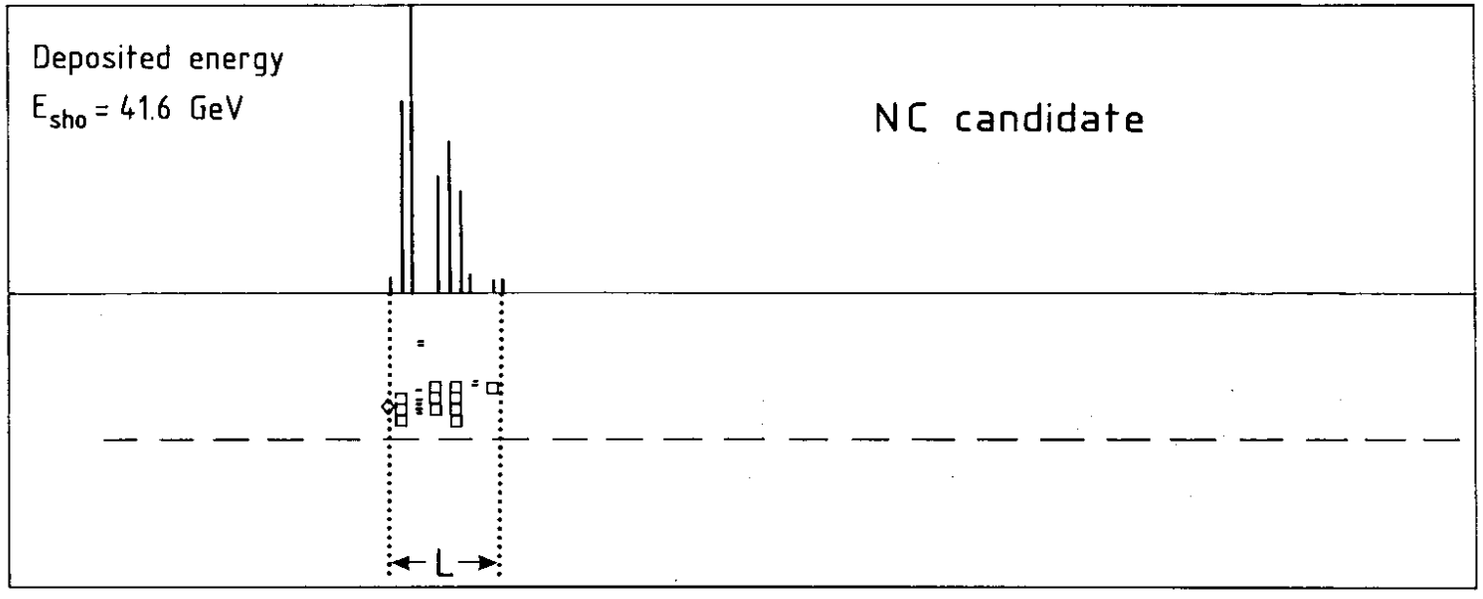
Deposited energy
E_{sho} = 41.6 GeV
NC candidate
L

Fig. 1

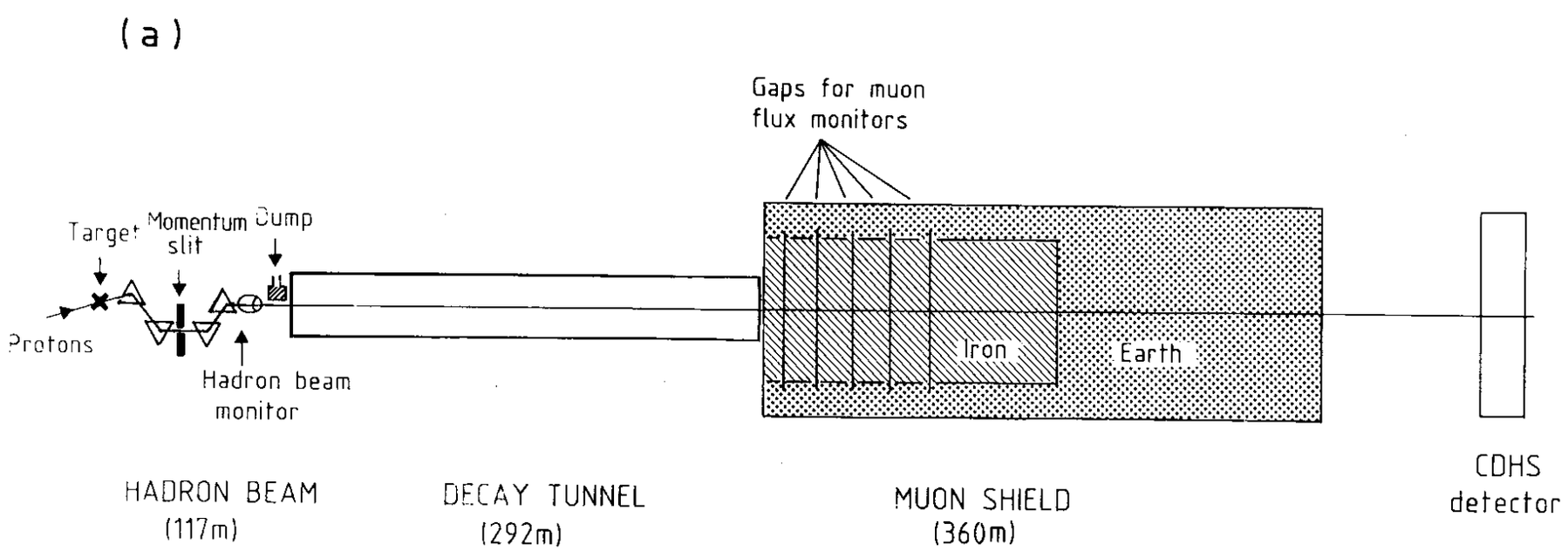
(a)
Gaps for muon flux monitors
Target
Momentum slit
Dump
Protons
Hadron beam monitor
Iron
Earth
CDHS detector
HADRON BEAM (117m)
DECAY TUNNEL (292m)
MUON SHIELD (360m)

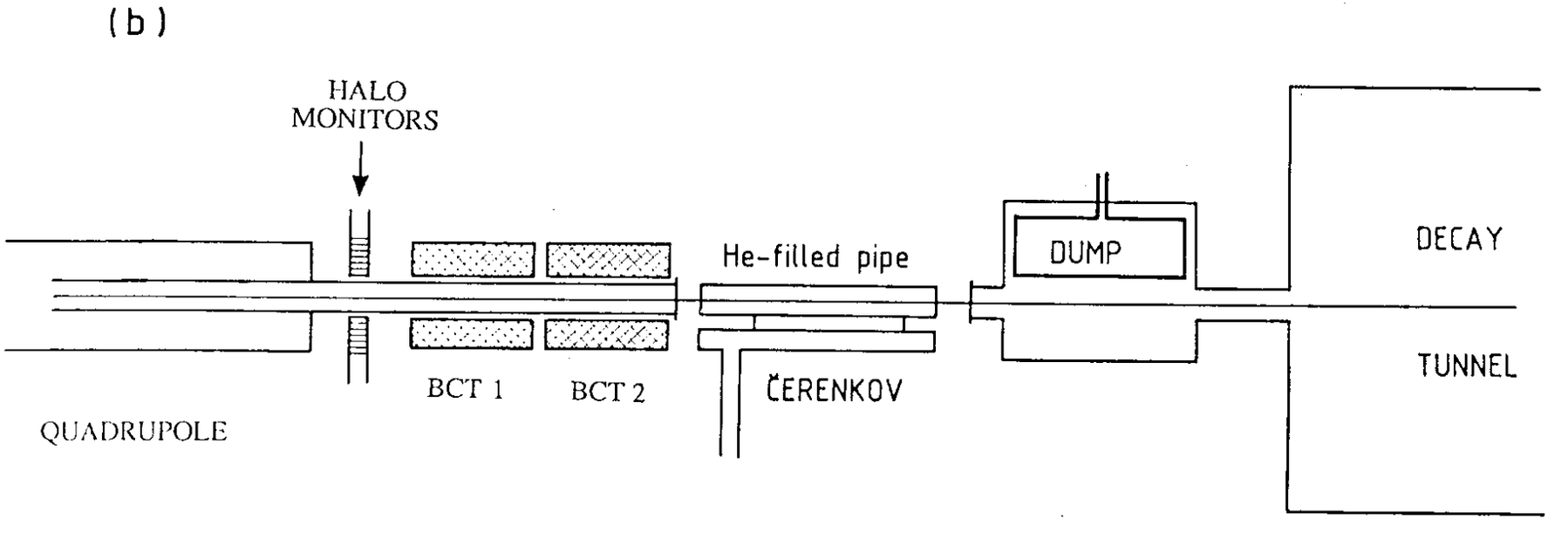
(b)
HALO MONITORS
He-filled pipe
DUMP
DECAY TUNNEL
BCT 1
BCT 2
ČERENKOV
QUADRUPOLE

Fig. 2

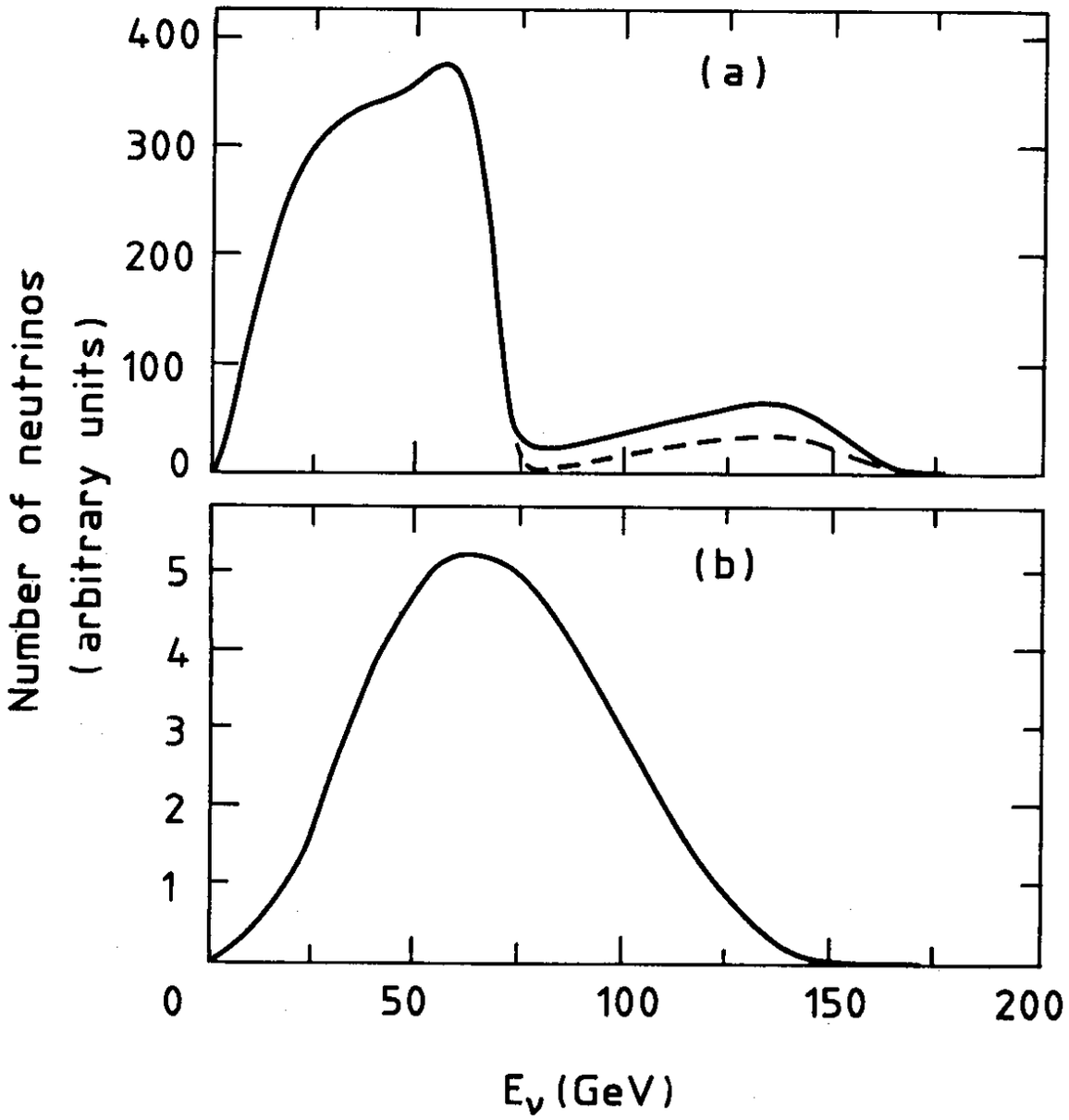
400
300
200
100
0
(a)
(b)
5
4
3
2
1
0
50
100
150
200
Number of neutrinos
(arbitrary units)
E_ν (GeV)

Fig. 3

(a)

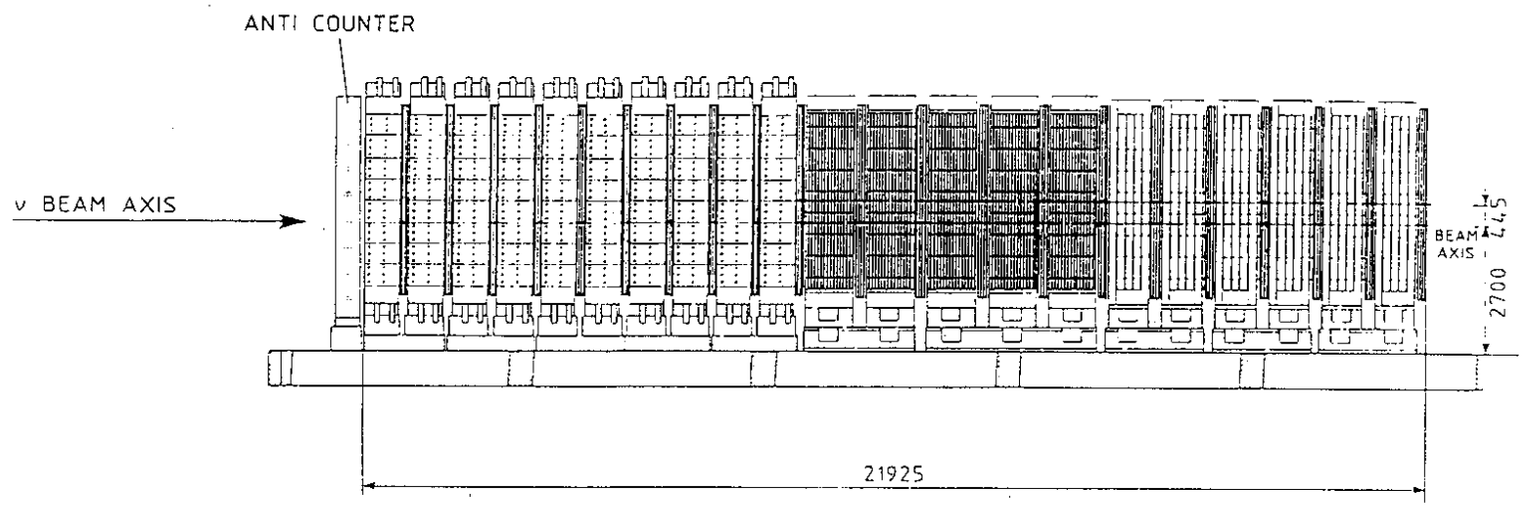
ANTI COUNTER
ν BEAM AXIS
BEAM AXIS
2700
445
21925

(b)

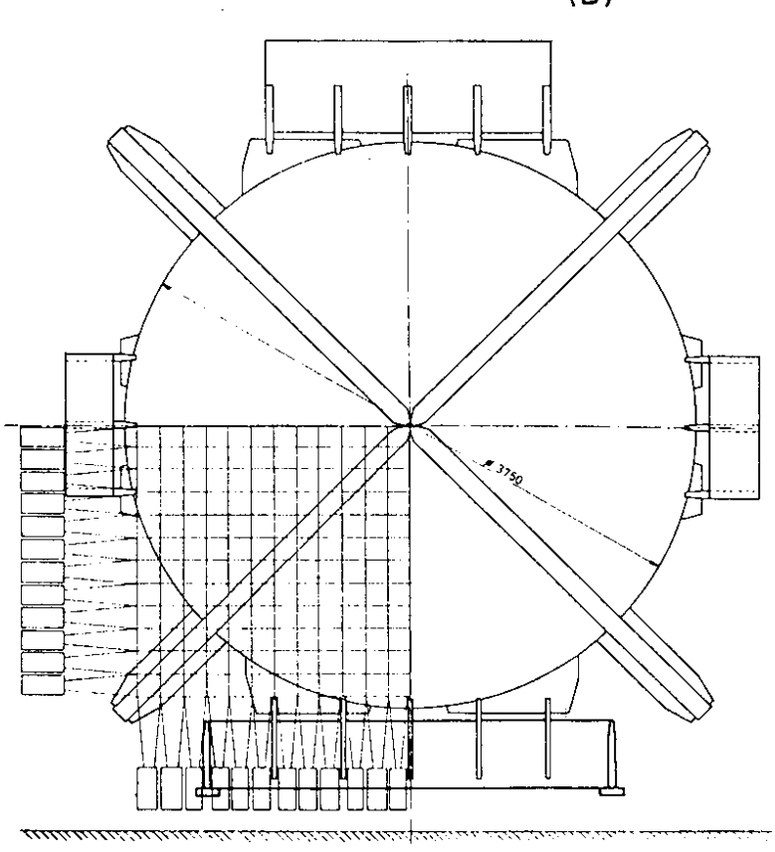
3750

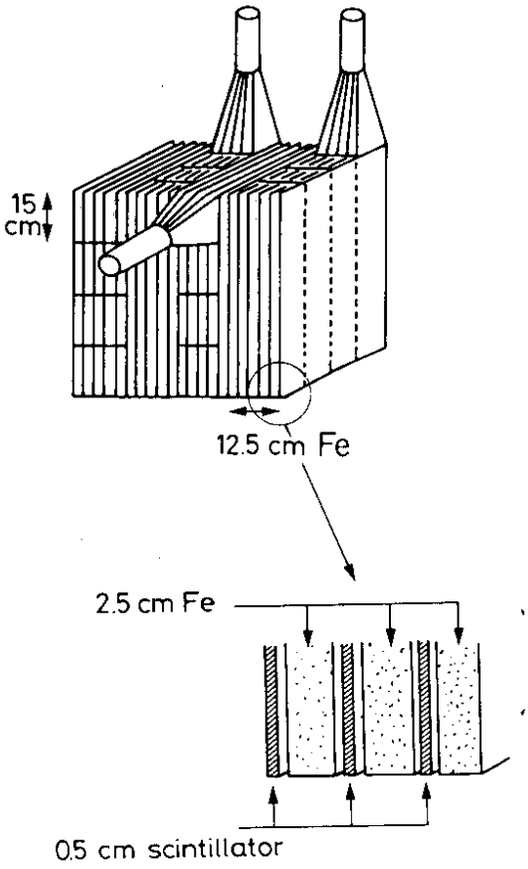
15 cm
12.5 cm Fe
2.5 cm Fe
0.5 cm scintillator

Fig. 4

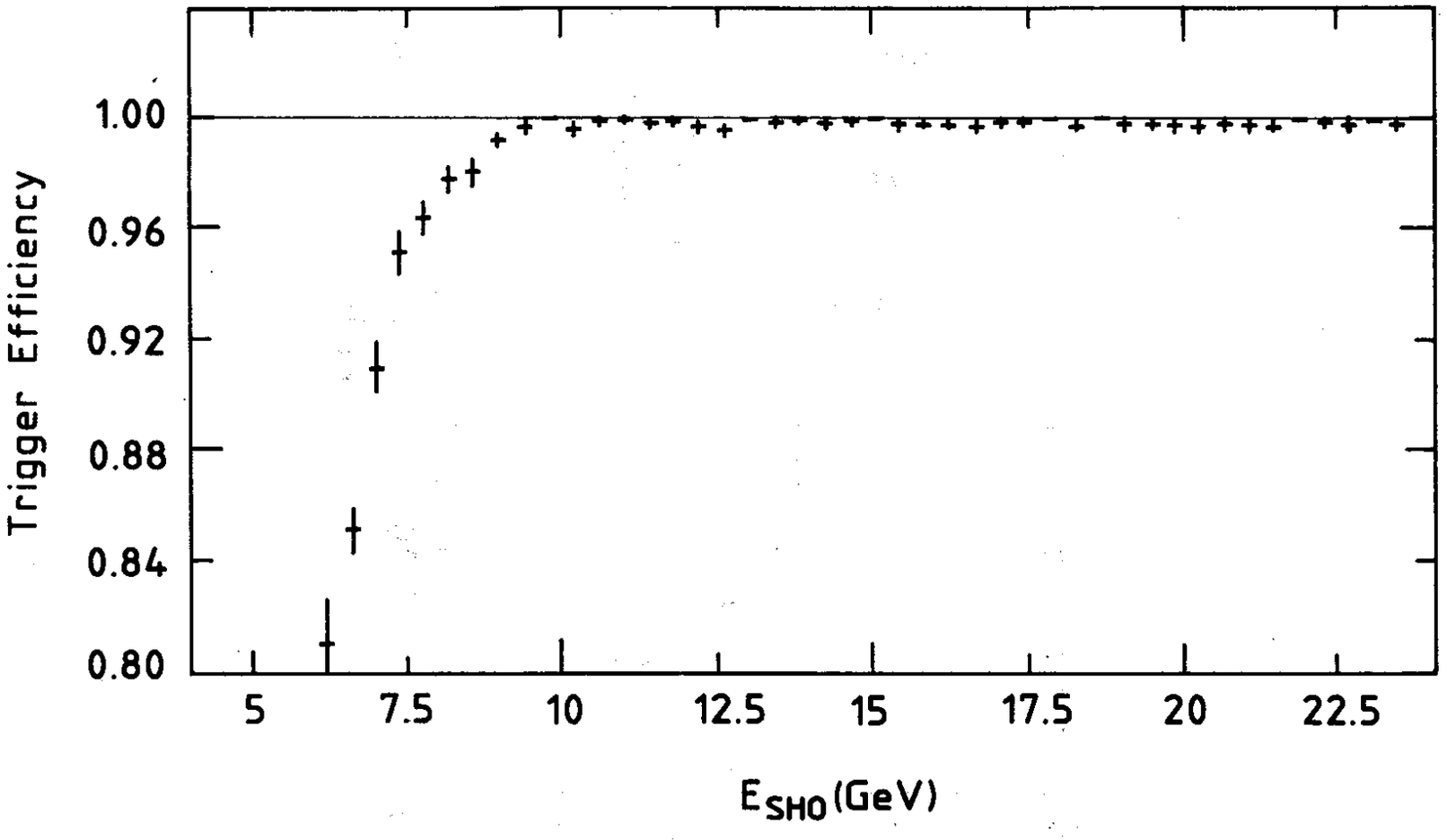
Trigger Efficiency
1.00
0.96
0.92
0.88
0.84
0.80
5
7.5
10
12.5
15
17.5
20
22.5
E_SHO (GeV)

Fig. 5

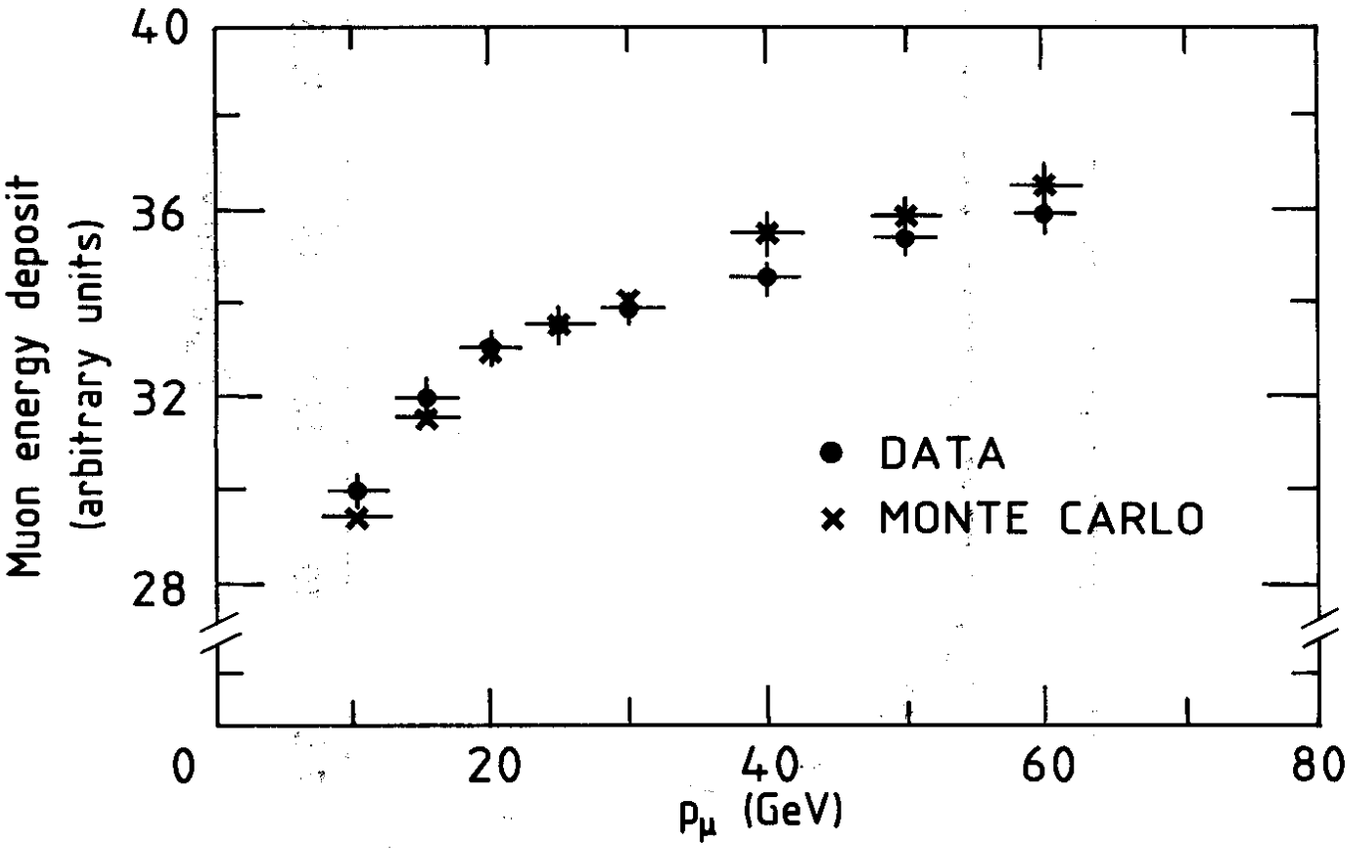
40
36
32
28
Muon energy deposit
(arbitrary units)
DATA
MONTE CARLO
0
20
40
60
80
p_μ (GeV)

Fig. 6

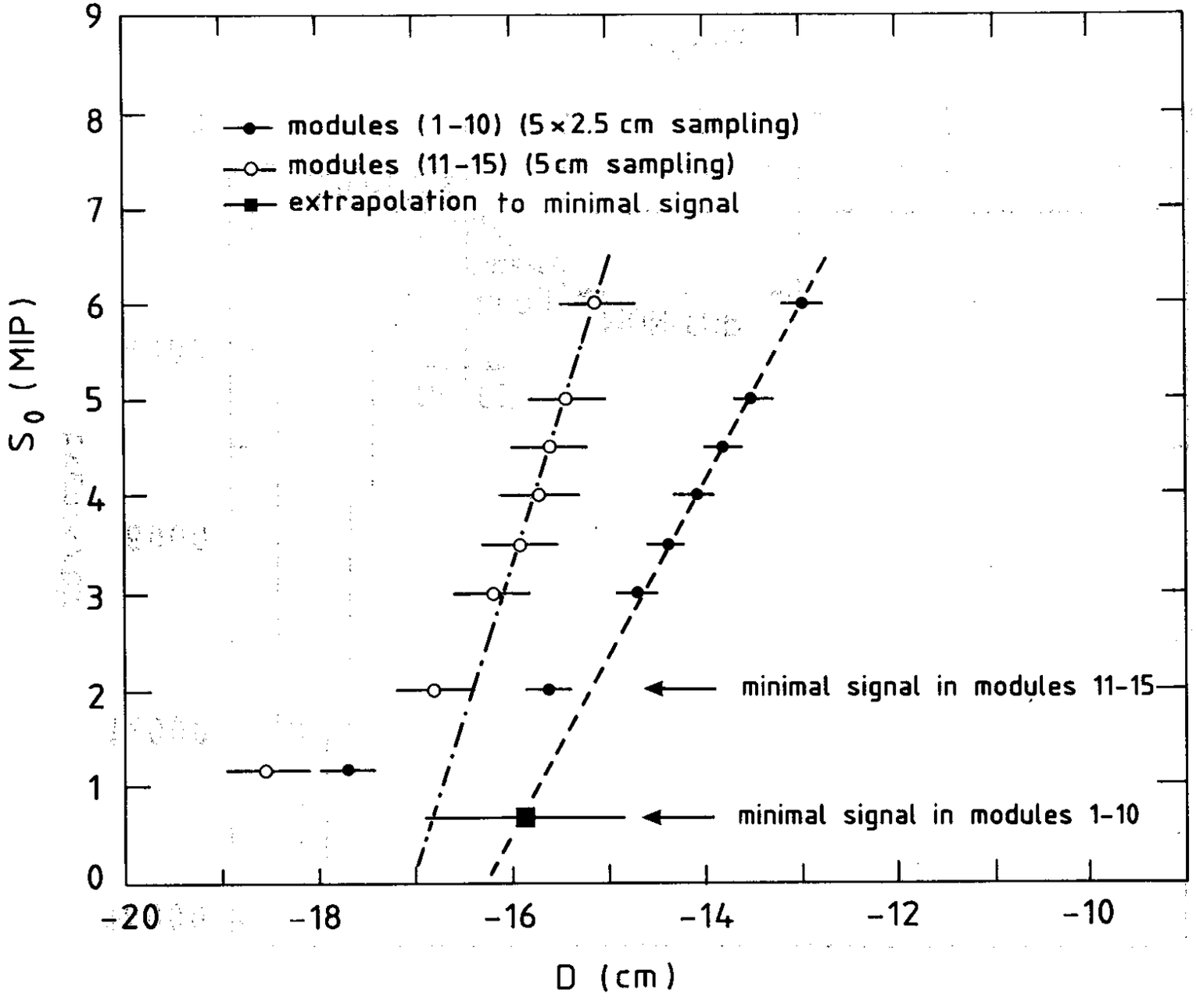
modules (1-10) (5×2.5 cm sampling)
modules (11-15) (5cm sampling)
extrapolation to minimal signal
minimal signal in modules 11-15
minimal signal in modules 1-10
S0 (MIP)
D (cm)
9
8
7
6
5
4
3
2
1
0
-20
-18
-16
-14
-12
-10

Fig. 7

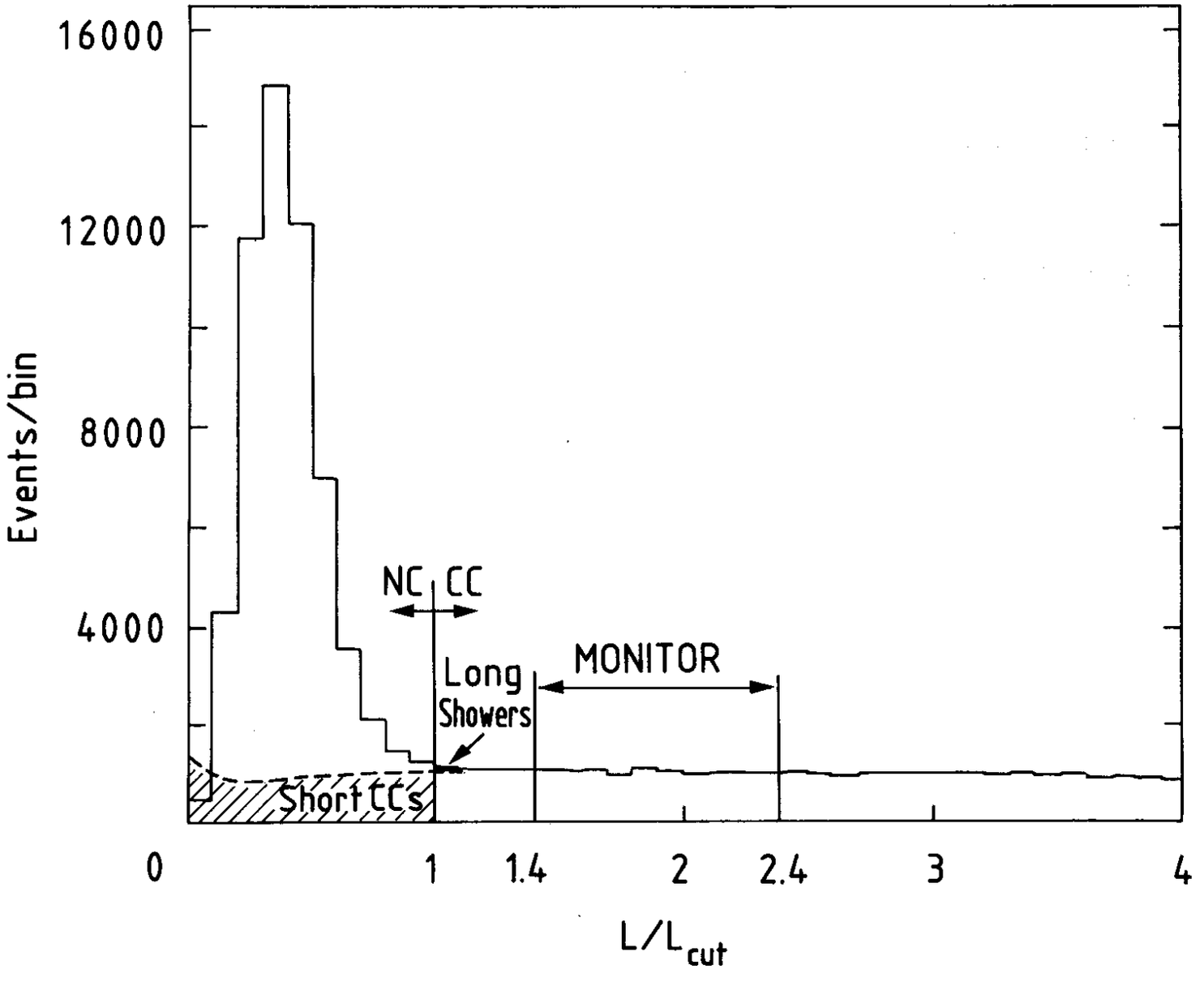
16000
12000
8000
4000
Events/bin
NC
CC
MONITOR
Long
Showers
Short CCs
0
1
1.4
2
2.4
3
4
L/L cut

Fig. 8

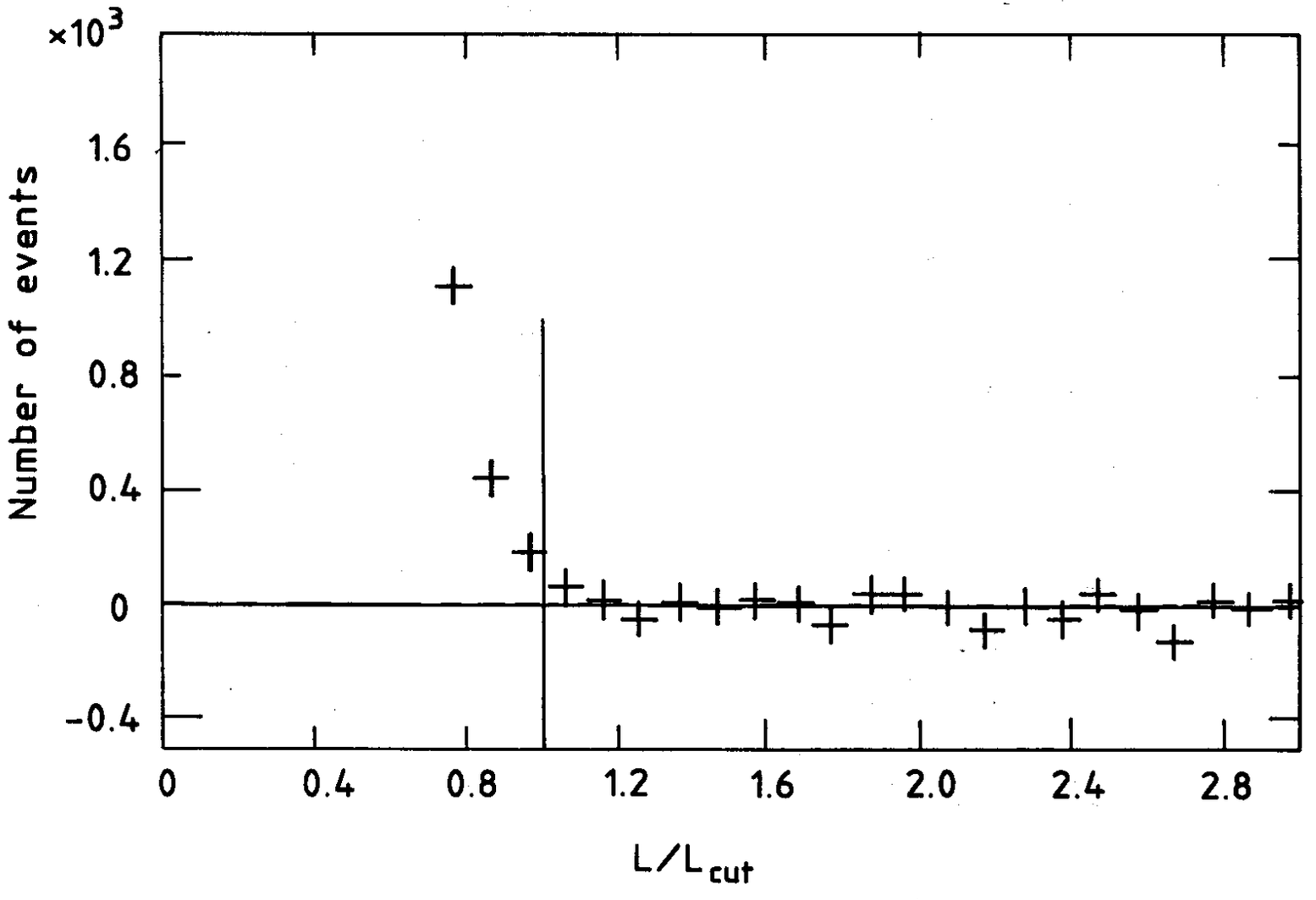

Fig. 9

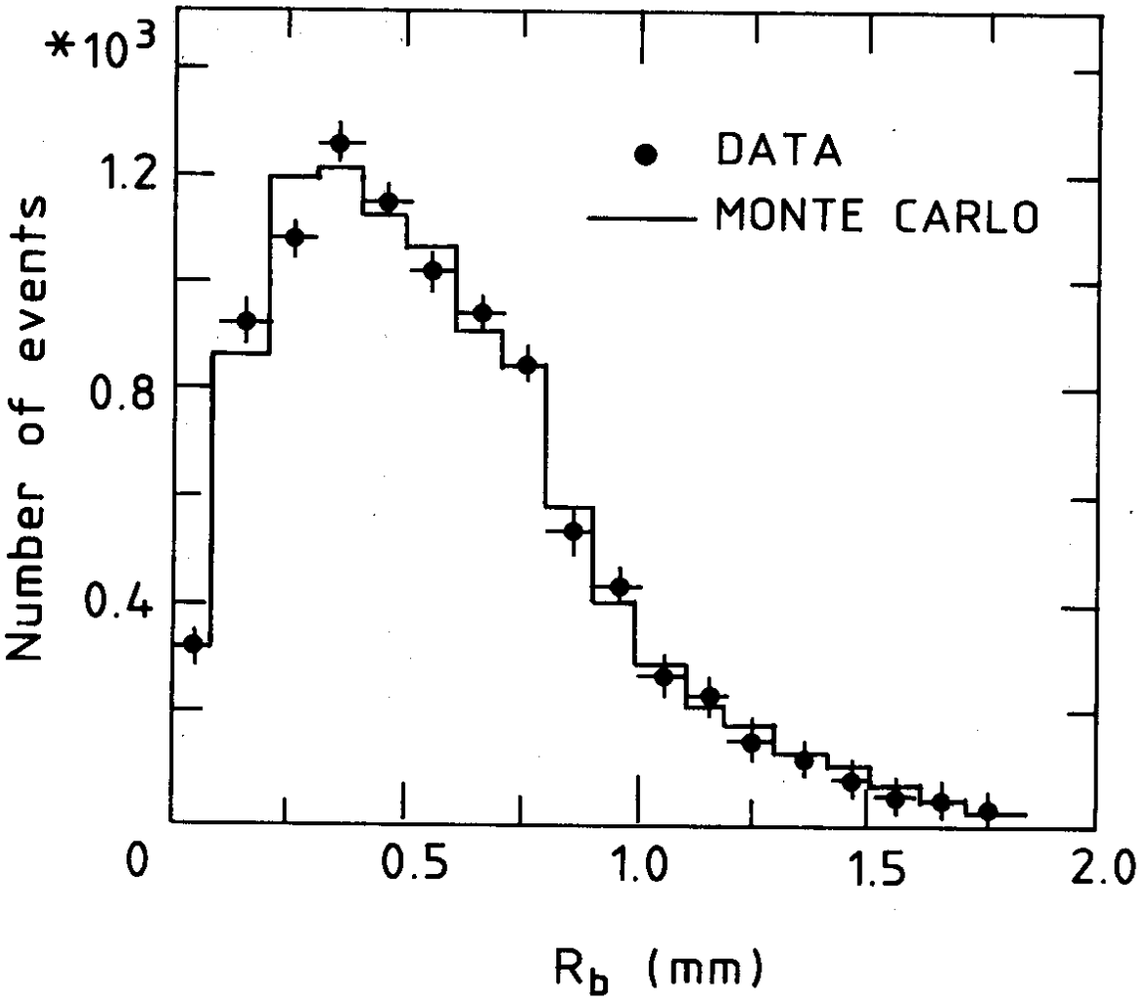
*10³
1.2
0.8
0.4
0
Number of events
DATA
MONTE CARLO
0.5
1.0
1.5
2.0
R_b (mm)

Fig. 10

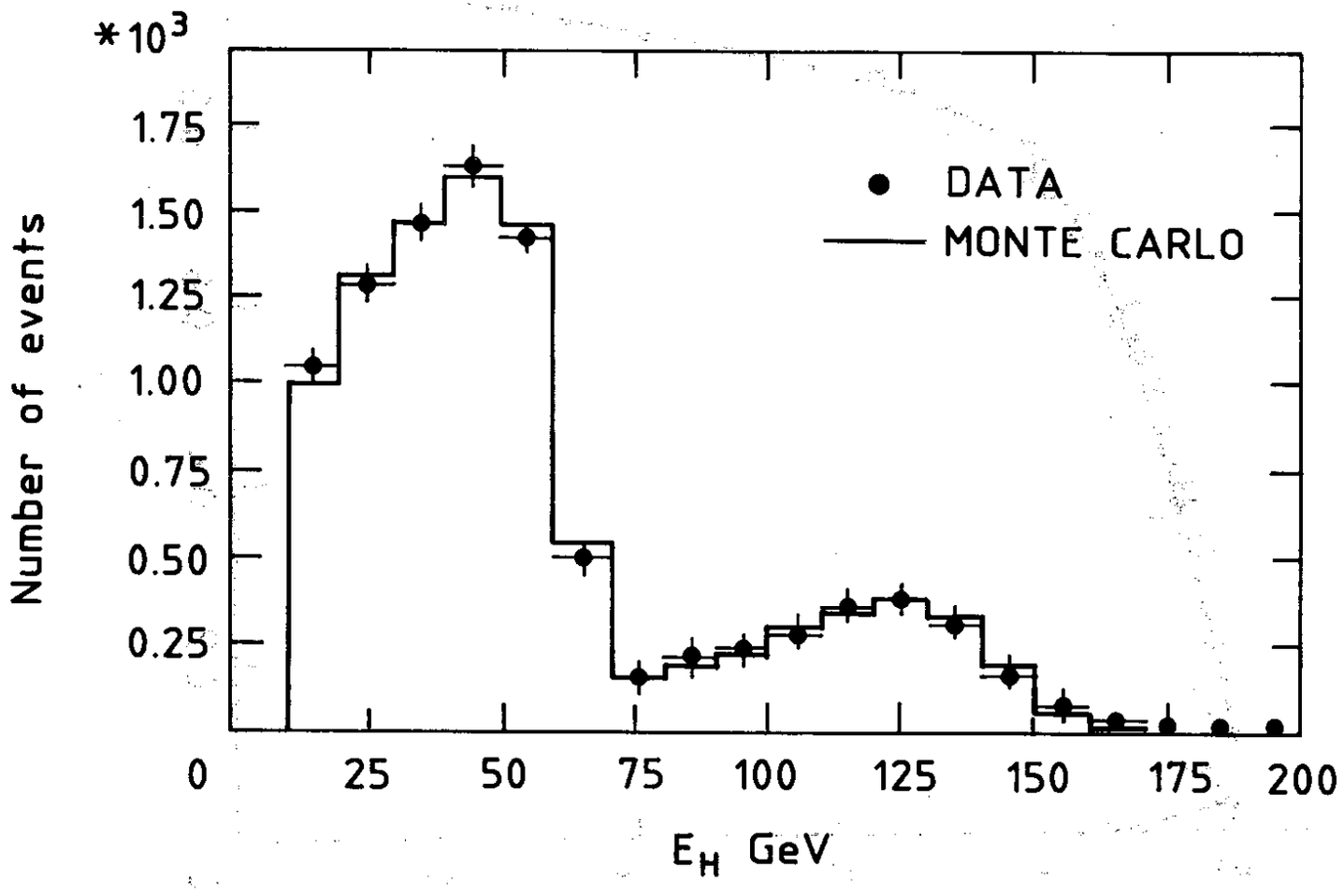
*10^3
1.75
1.50
1.25
1.00
0.75
0.50
0.25
Number of events
DATA
MONTE CARLO
0
25
50
75
100
125
150
175
200
E_H GeV

Fig. 11

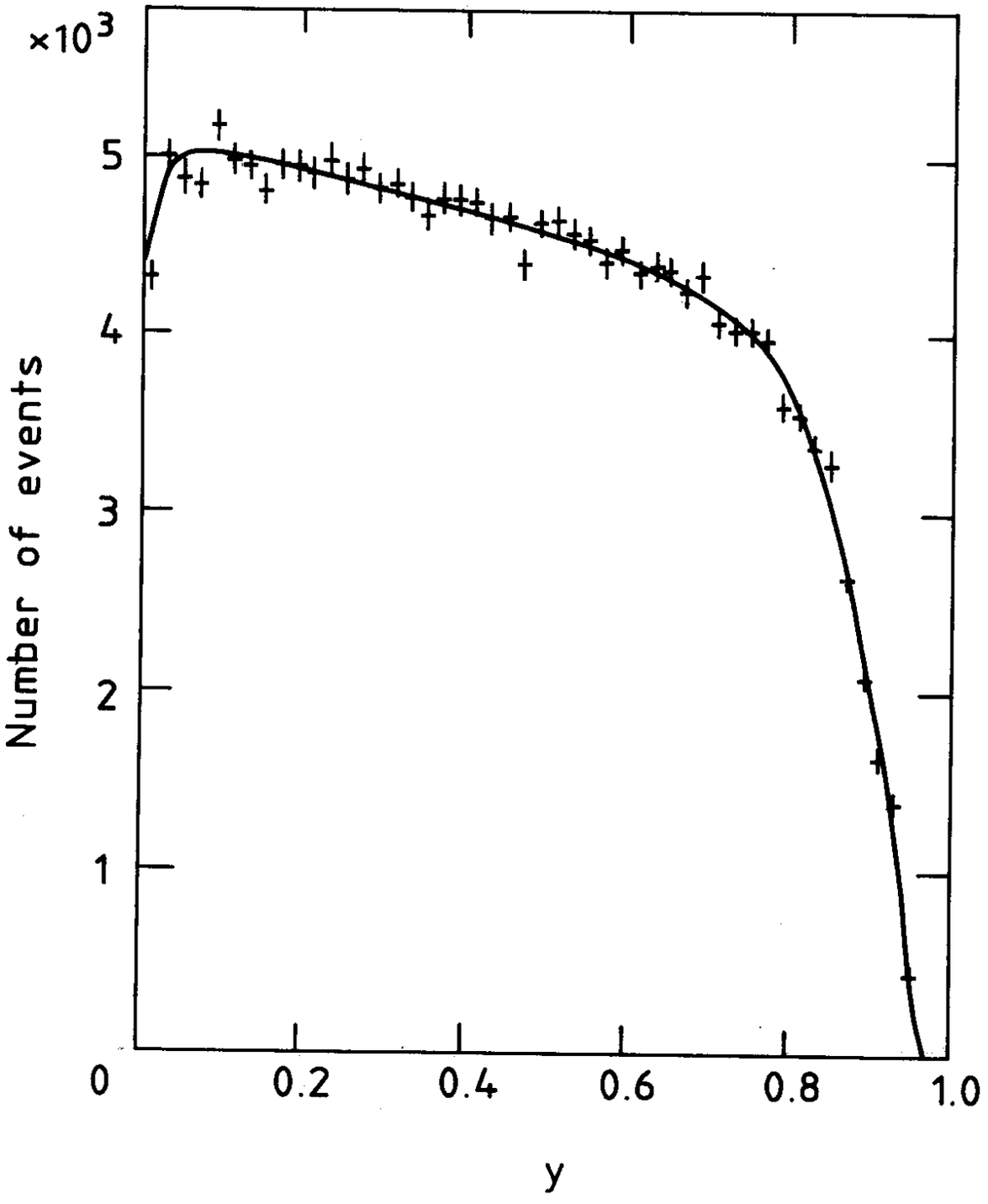

Fig. 12

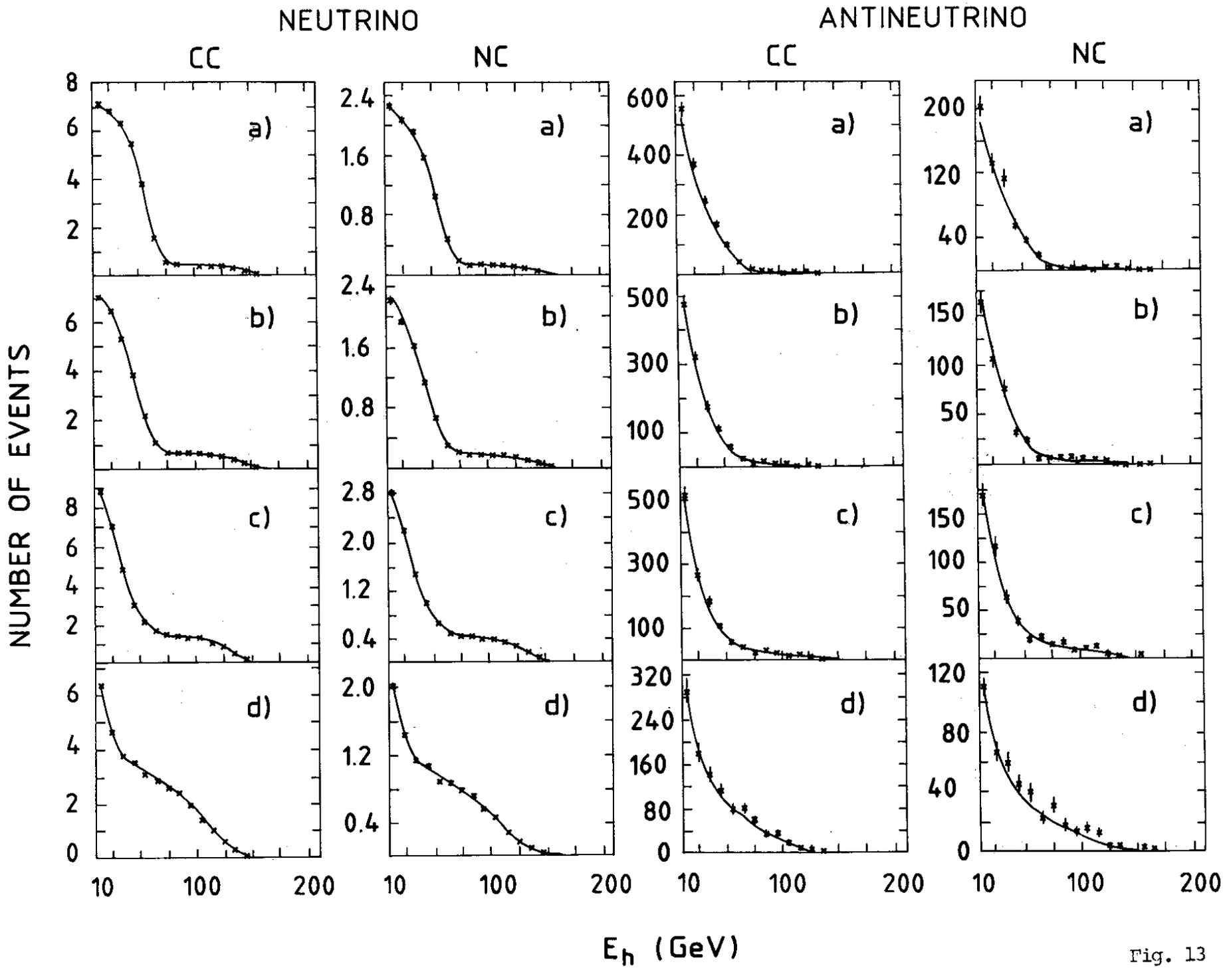
NEUTRINO
ANTINEUTRINO
CC
NC
CC
NC
a)
b)
c)
d)
NUMBER OF EVENTS
E_h (GeV)
10
100
200

Fig. 13

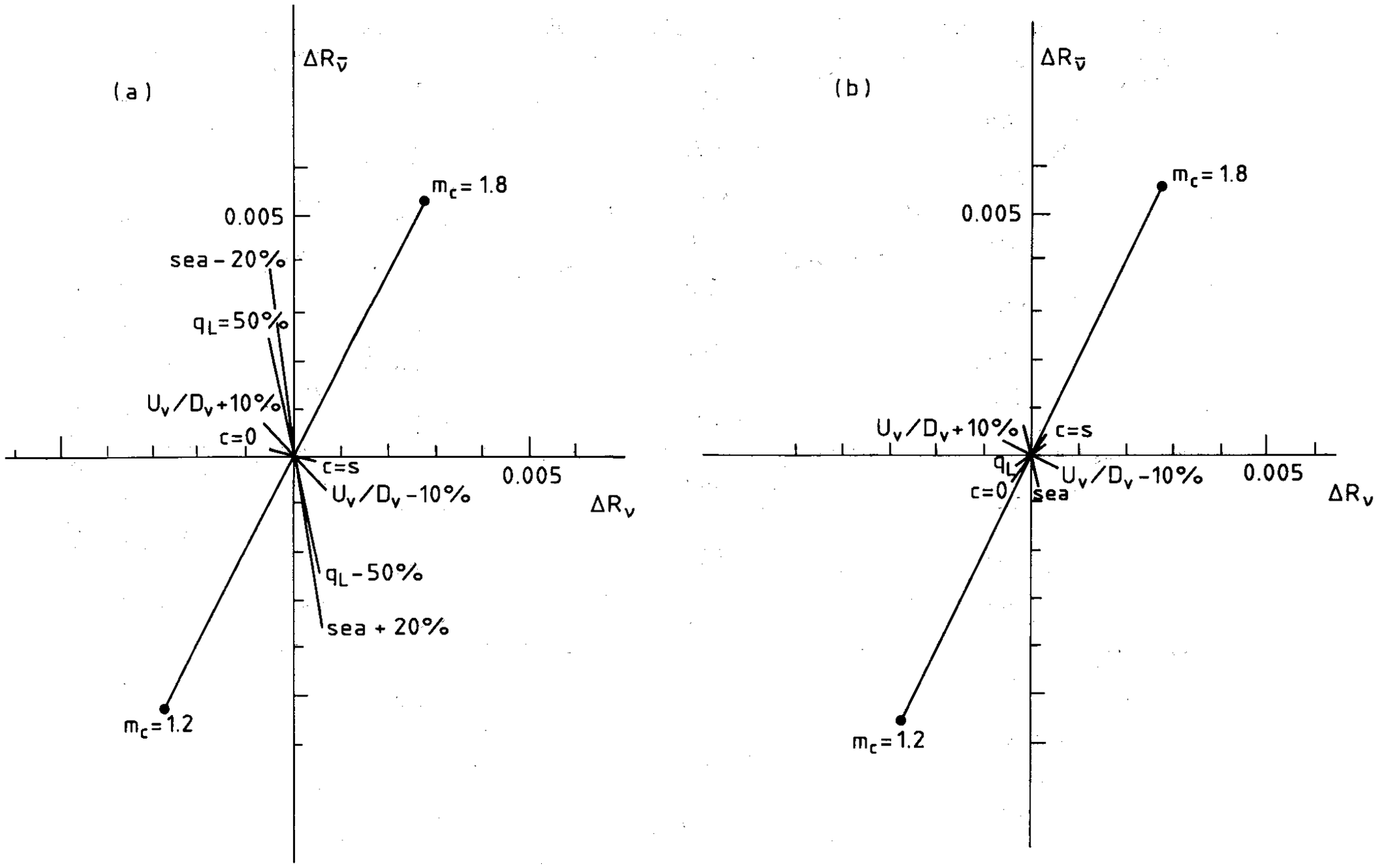
(a)
$\Delta R_{\bar{v}}$
$m_c = 1.8$
0.005
sea − 20%
q_L = 50%
U_v/D_v +10%
c=0
c=s
U_v/D_v −10%
0.005
ΔR_v
q_L − 50%
sea + 20%
$m_c = 1.2$
(b)
$\Delta R_{\bar{v}}$
$m_c = 1.8$
0.005
U_v/D_v +10%
c=s
q_L
U_v/D_v −10%
0.005
c=0
sea
ΔR_v
$m_c = 1.2$

Fig. 14

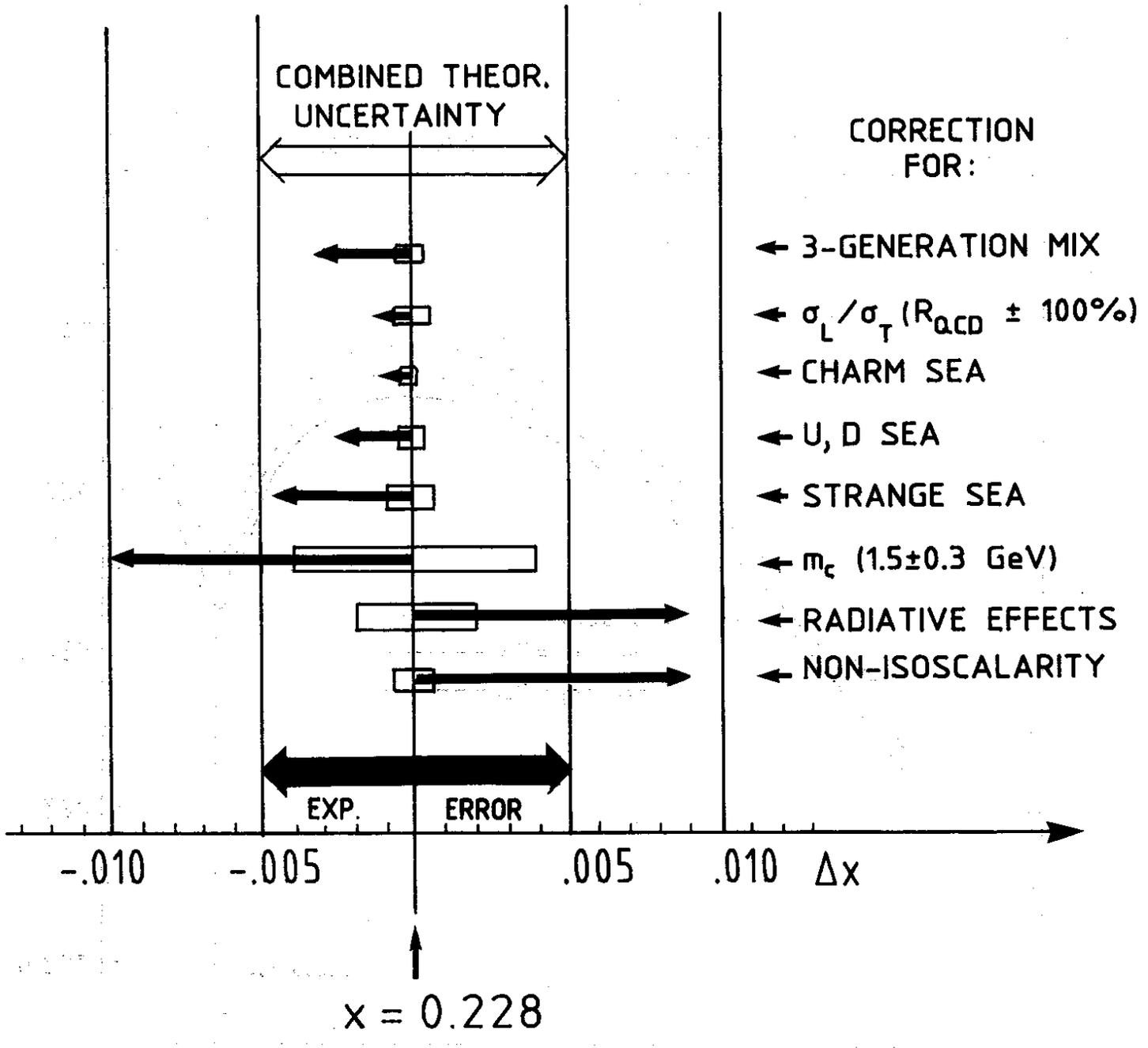
COMBINED THEOR.
UNCERTAINTY
CORRECTION
FOR:
3-GENERATION MIX
σ_L/σ_T (R_{QCD} ± 100%)
CHARM SEA
U, D SEA
STRANGE SEA
m_c (1.5±0.3 GeV)
RADIATIVE EFFECTS
NON-ISOSCALARITY
EXP.
ERROR
-.010
-.005
.005
.010
Δx
x = 0.228

Fig. 15

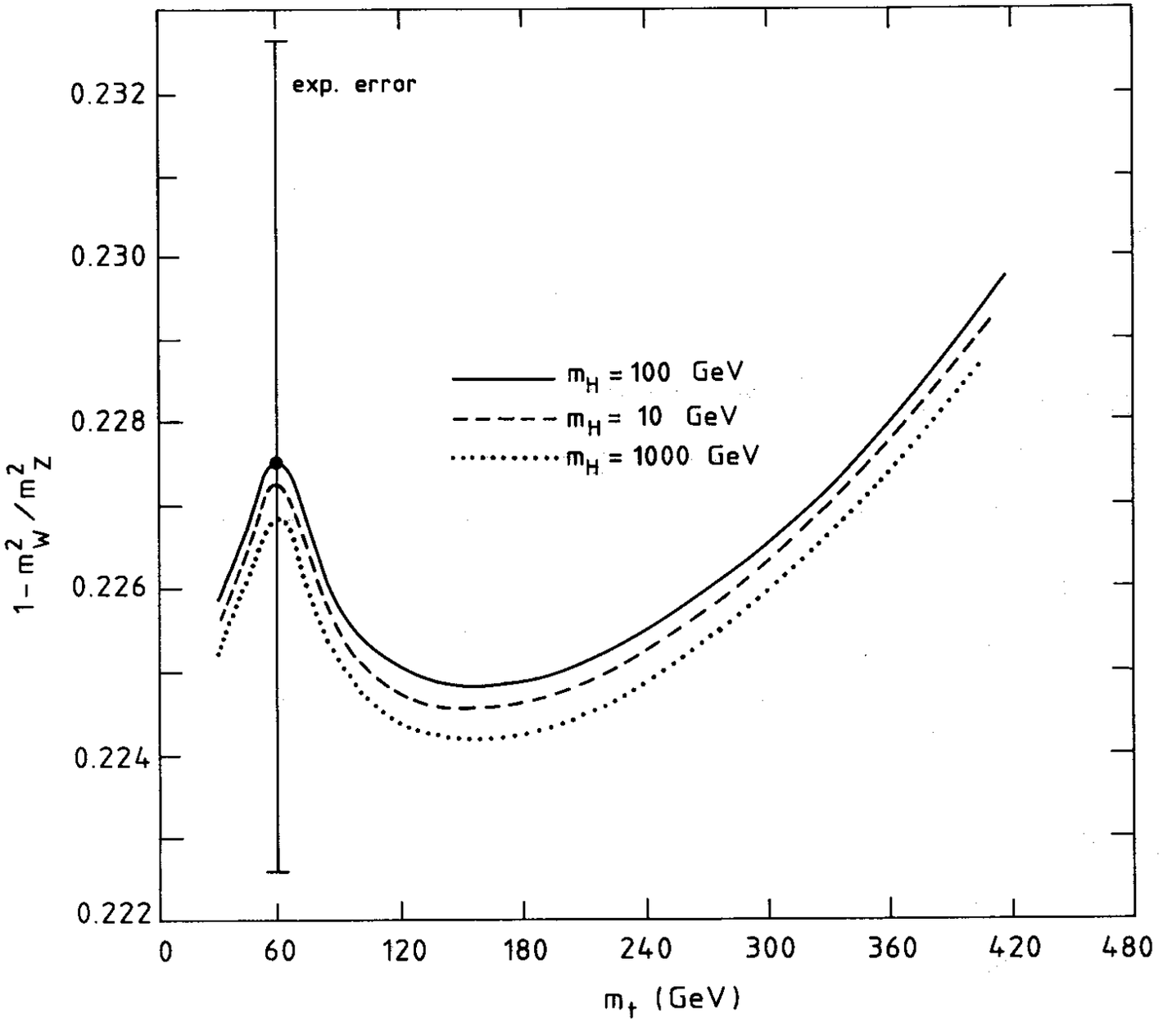
exp. error
m_H = 100 GeV
m_H = 10 GeV
m_H = 1000 GeV
$1 - m_W^2 / m_Z^2$
0.232
0.230
0.228
0.226
0.224
0.222
0
60
120
180
240
300
360
420
480
m_t (GeV)

Fig. 16

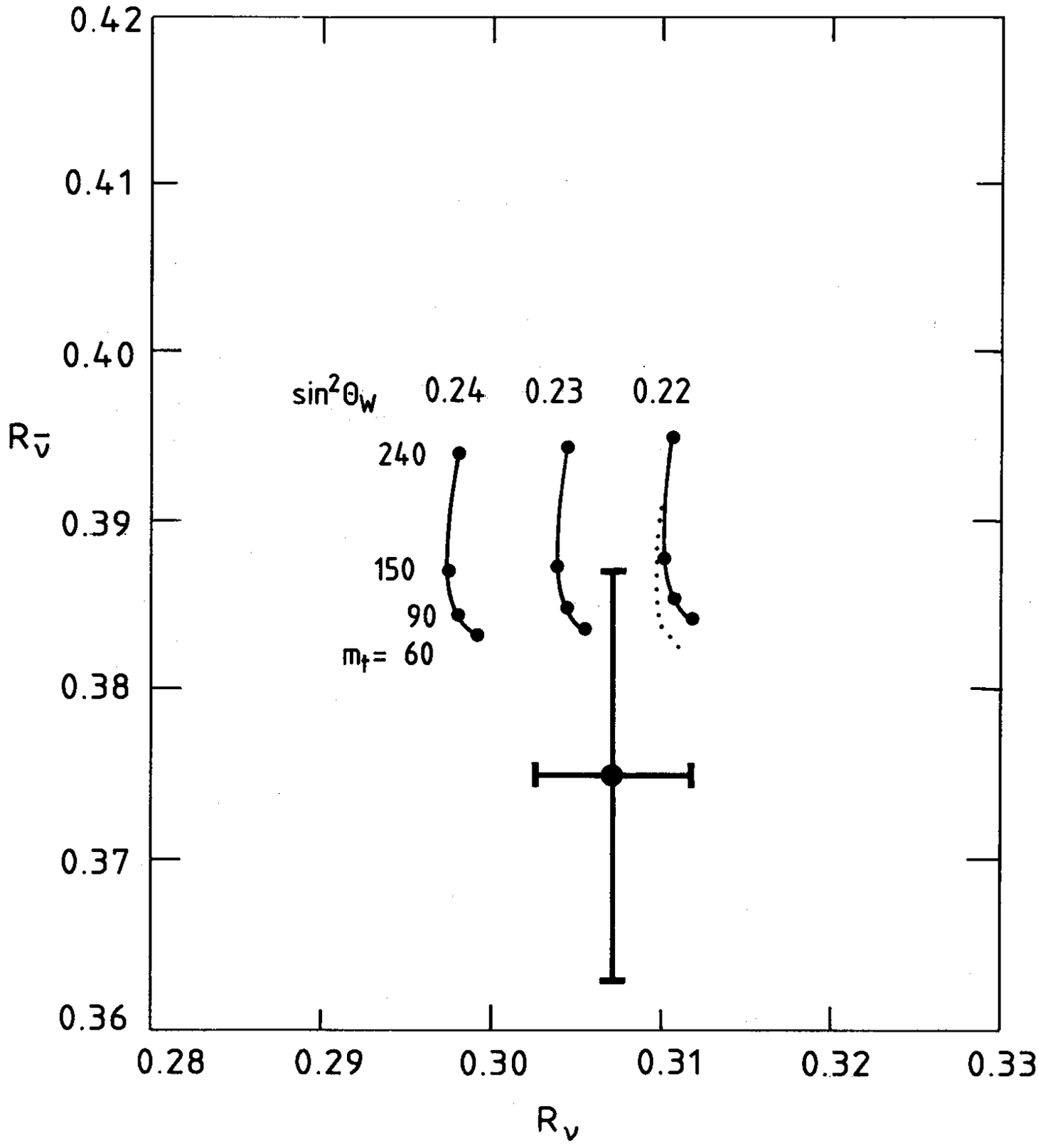
0.42
0.41
0.40
0.39
0.38
0.37
0.36
$R_{\bar{\nu}}$
$\sin^2\theta_W$ 0.24 0.23 0.22
240
150
90
m_t= 60
0.28
0.29
0.30
0.31
0.32
0.33
R_ν

Fig. 17

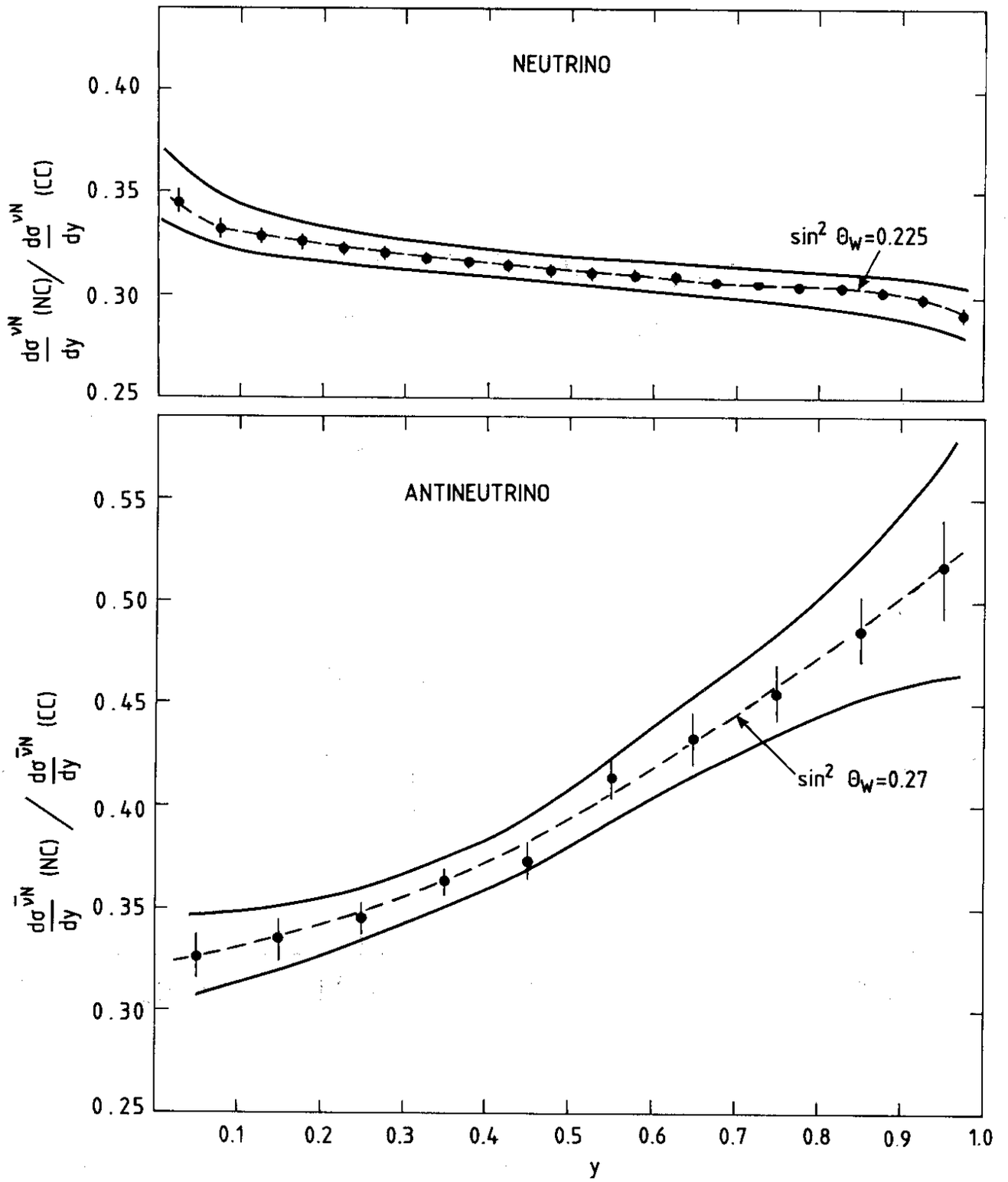
NEUTRINO
$\frac{d\sigma^{\nu N}(NC)}{dy} / \frac{d\sigma^{\nu N}(CC)}{dy}$
$\sin^2 \theta_W = 0.225$
0.40
0.35
0.30
0.25
ANTINEUTRINO
$\frac{d\sigma^{\bar{\nu} N}(NC)}{dy} / \frac{d\sigma^{\bar{\nu} N}(CC)}{dy}$
$\sin^2 \theta_W = 0.27$
0.55
0.50
0.45
0.40
0.35
0.30
0.25
0.1
0.2
0.3
0.4
0.5
0.6
0.7
0.8
0.9
1.0
y

Fig. 18

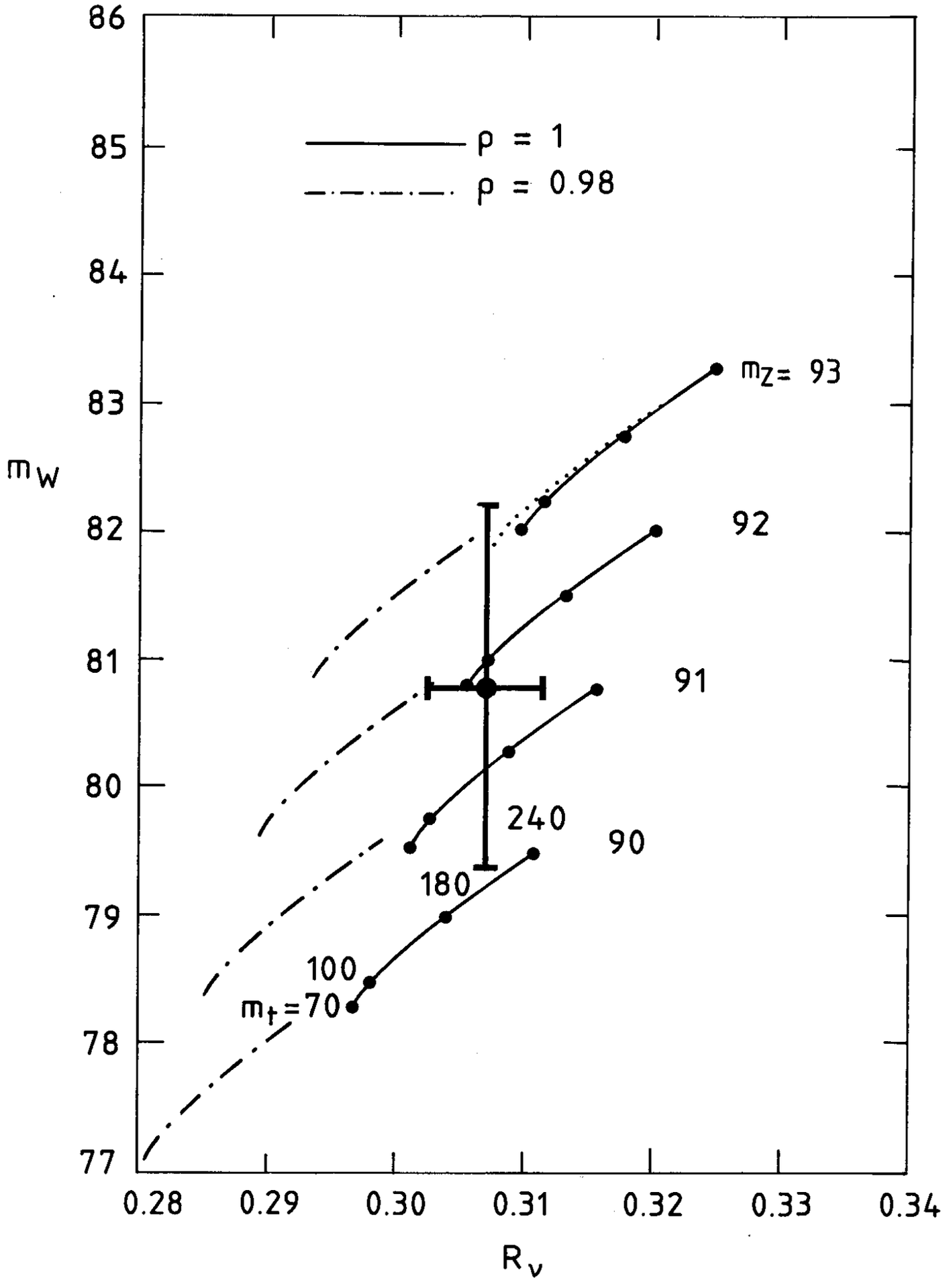
ρ = 1
ρ = 0.98
m_Z= 93
92
91
90
240
180
100
m_t=70
m_W
R_ν
86
85
84
83
82
81
80
79
78
77
0.28
0.29
0.30
0.31
0.32
0.33
0.34

Fig. 19